



NTNU – Trondheim
Norwegian University of
Science and Technology

Filament winding of composite tubes

Karsten Dons

Master of Science in Mechanical Engineering

Submission date: June 2013

Supervisor: Andreas Echtermeyer, IPM

Norwegian University of Science and Technology
Department of Engineering Design and Materials

THE NORWEGIAN UNIVERSITY
OF SCIENCE AND TECHNOLOGY
DEPARTMENT OF ENGINEERING DESIGN
AND MATERIALS

**MASTER THESIS SPRING 2013
FOR
STUD. TECHN. KARSTEN DONS**

Filament winding of composite tubes

Vikling av komposittrør

Pressure vessels and pipes are important applications in many industries, such as offshore, chemical, automotive, aerospace. One of the most suitable processing methods for these composites is the filament winding process. This is an automated method to create composite material components.

This project shall explore new methods to wind composite tubes by combining fiber strands and mats. Focus will be put on producing the terminations of the tubes. The work will be related to process development, strength calculations, finite element analysis and testing of the components made.

The thesis should include the signed problem text, and be written as a research report with summary both in English and Norwegian, conclusion, literature references, table of contents, etc. During preparation of the text, the candidate should make efforts to create a well arranged and well written report. To ease the evaluation of the thesis, it is important to cross-reference text, tables and figures. For evaluation of the work a thorough discussion of results is appreciated. Safety evaluations for experimental work shall be added to the Appendix.

Three weeks after start of the thesis work, an A3 sheet illustrating the work is to be handed in. A template for this presentation is available on the IPM's web site under the menu "Masteroppgave" (<http://www.ntnu.no/ipm/masteroppgave>). This sheet should be updated one week before the Master's thesis is submitted.

The thesis shall be submitted electronically via DAIM, NTNU's system for Digital Archiving and Submission of Master's thesis.



Torgeir Welo
Head of Division



Andreas Echtermeyer
Professor/Supervisor



NTNU
Norges teknisk-
naturvitenskapelige universitet
Institutt for produktutvikling
og materialer

NORGES TEKNISK NATURVITENSKAPELIGE UNIVERSITET

Institutt for Produktutvikling og Materialer

Sammendrag

Vikling av komposittrør

av Karsten DONS

Kompositter har mange fordelaktige egenskaper i forhold til tradisjonelle rørmaterialer, men mangelen på enkle og holdbare endestykker har begrenset bruken i trykksatte systemer. En ny type endestykke har blitt designet, produsert og testet i denne oppgaven. Endestykket består av to hoveddeler, en boltet forbindelse med radielt plasserte bolter og et spesiallaget komposittrør. Røret er forsterket med fibermatter i endene for å være egnet for en boltet forbindelse. I tillegg har en vellykket produksjonsmetode som involverer vikling og fibermatter blitt utviklet. To tester av det produserte røret ble utført: en trykktest og en strekktest. Trykktesten ble ikke fullført ettersom røret startet å lekke. I strekktesten ble den lineære last grensen målt til 67,2 kN og maksimal last 96,2 kN. Resultatene stemmer svært godt med den predikerte styrken. Det kan konkluderes med at forsterkning med fibermatter og en radiell bolt forbindelse er en lovende løsning.

Abstract

Filament winding of composite tubes

by Karsten DONS

Composite tubes outperform traditional pipe materials in applications requiring low weight, corrosion resistance and high strength. However, the lack of simple and reliable end fittings have limited their use. A new end fitting design for composite tubes have been designed, produced and tested. The end fitting consist of two main parts, a bolted connection with radially placed bolts and a custom made composite tube. The tube is reinforced in the ends with fiber mats to achieve a layup suitable for a bolted connection. In addition a production method involving filament winding and fiber mats has successfully been developed. Two tests of the produced tube were performed: an internal pressure test and a tensile test. During the pressure test, the tube leaked at a low pressure and the quality of the end fitting could not be determined. Axial strength was tested with a tensile test and a very good result was obtained. The linear load limit was found to be 67,2 kN and the maximum axial load was 96,2 kN. This is in good agreement with the predictions. It was concluded that this new end fitting design is a promising solution for composite tube junctions.

Contents

Task Description	i
Sammendrag	ii
Abstract	iii
Table of Contents	iv
List of Figures	ix
List of Tables	xiii
Preface	xv
1 Introduction	1
1.1 Introduction	1
1.2 End fitting physics	2
1.3 Previously suggested end fittings	3
1.4 New design proposed by Prof. Echtermeyer, NTNU	5
1.5 Introduction to bolted joint geometry	6
1.6 Failure modes of bolted joints	8
1.7 Recommendations for bolted joint geometry	9
1.7.1 Handbook of composites	9
1.7.2 Composite Design	10
1.7.3 Composite airframe structures	10
1.7.4 A design methodology for mechanically fastened joints in laminated composite materials	10

1.7.5	Effect of stacking sequence and clamping force on the bearing strengths of mechanically fastened joints in composite materials	11
1.8	Applicable standards	11
1.9	Winding or fiber angle definition	12
1.10	Laminate theory	12
1.10.1	Maximum stress criterion	14
2	End fitting design	15
2.1	Design requirements and limitations for the sample tube	15
2.2	Hub design	16
2.2.1	Sealing	17
2.3	Material properties	17
2.4	Middle section layup	19
2.5	Load distribution	20
2.5.1	Bearing load	21
2.5.2	Net section load	22
2.5.3	Shear out load	22
2.5.4	Wedge splitting load	22
2.5.5	Combined failure	23
2.6	Number of bolts and bolt diameter	23
2.7	Edge distance	25
2.8	Transition area	26
2.9	Bolt area layup	26
2.10	Laminate theory	29
2.11	Sample tube geometry and stagger distance	32
2.12	Bushings and bolt shear	33
2.13	Limitations	36
3	Tube and end fitting production	37
3.1	Filament Winding	37
3.2	Tube and end fitting production	39
3.3	End fitting connection	43
3.4	Liner	44
3.5	Geometric measuring of finished tube	45
3.6	Microscopy of cross sections	47
3.7	Fiber volume fraction	48
3.7.1	Scaling of material properties	50
3.8	Laminate theory	51

4	FEA model	53
4.1	Geometry, elements, mesh and solver	53
4.2	Layup and material properties	54
4.3	Loads, boundary conditions and solving method	55
4.4	Output	56
4.5	Force and displacement scaling	56
5	Experimental testing	57
5.1	Instrumentation	57
5.1.1	Center part	58
5.1.2	Bolt area	59
5.1.3	Transition area	61
5.2	Pressure test	61
5.3	Tensile test	61
5.3.1	Test setup	62
5.3.2	Strain rate	63
6	Results	65
6.1	FEA modeling	65
6.2	Pressure test	67
6.3	Tensile test	68
6.4	Strain measurements	71
6.5	Center part	71
6.6	Bolt area	73
6.7	Axial strain, from tube edge to tube center	76
6.8	Transition area	78
6.9	Comparison between FEA and Experimental results	78
7	Discussion	81
7.1	Production	81
7.2	Pressure test	82
7.2.1	Leakage	82
7.3	Tensile test	82
7.4	Center part	84
7.5	Bolt area	85
7.6	Transition area	86
7.7	FEA model compared to experimental results	87
8	Conclusion	89

8.1	Production method	89
8.2	Experimental	90
8.3	Further work and suggested improvements to the design . . .	90
 Bibliography		 92
 A Tables		 99
B Hub drawing		105
C FEA shell drawing		107
D HSE forms		109

List of Figures

1.1	End fitting physics	2
1.2	Patents	4
1.3	Idea illustration	5
1.4	Joint geometry for a single row joint.	7
1.5	Simplified drawing of a bolted connection. Figure adapted from Chamis [1].	8
1.6	Failure modes. Figure adapted from Chamis [1].	8
1.7	Winding angle Θ . Figure adapted from Messenger et al. [2].	12
2.1	Relative failure strength vs. p/d.	24
2.2	Ply drop off. Adapted from Mukherjee and Varughese [3]	26
2.3	Tube geomerty, as made on mandrel.	34
2.4	Bushing test setup. Photo by Kaspar Lasn.	35
3.1	Filament winding, resin bath to the left, winding head and mandrel.	38
3.2	Mat application	39
3.3	Helical winding over a mat.	40
3.4	Finished tube before cutting.	42
3.5	Bolt hole drilling	42
3.6	Bolt assembly. From the top: Hub, bushing, washers, screw head.	43
3.7	Finished tube and end fitting	44
3.8	Cross section and specimen location on produced tube.	44
3.9	Microscopy of a helical ply wound over a mat edge. Inside of tube to the bottom of the photo.	47
3.10	Microscopy of cross section. Inside of tube to the bottom of the photo.	48
3.11	Burnt off test sample	49

4.1	Mesh around bolt hole.	54
4.2	FEA model; Axial edge along red line and net section along green line.	54
4.3	Bolt hole coordinate system. Figure adapted from Aktas and Husnu Dirikolu [4]	55
5.1	Instrumentation areas.	58
5.2	Strain gauges T1-T7, C0, CA45 and CA90. Strain gauges illustrated as squares.	59
5.3	Placement of optical fiber between bolt holes. The fiber was glued to the tube along the black lines.	60
5.4	Strain gauges BH1-BH4 around a bolt hole.	60
5.5	Pressure test setup.	62
5.6	Modified end fitting for tensile test, with optical fiber glued on.	63
5.7	Tensile test setup.	64
6.1	Strain in axial direction at a crosshead displacement of 0,8 mm.	65
6.2	Strain in hoop direction at a crosshead displacement of 0,8 mm.	66
6.3	Axial strain in one net section between two bolts at a crosshead displacement of 0,8 mm.	66
6.4	Pressure vs. time.	67
6.5	Stresses in hoop direction at transition area.	67
6.6	Bolts under load at a crosshead displacement of 11,3 mm.	68
6.7	Bolt and tube after unloading.	69
6.8	Force and crosshead displacement vs. time	69
6.9	Force vs. crosshead displacement.	70
6.10	Axial strain at the center vs. displacement.	72
6.11	Strain for CA 45, 135, 224 and 315 normalized by the average strain vs. displacement.	72
6.12	Strain at BH2 and BH4 plotted against displacement together with force scaled FEA results.	73
6.13	Strain in axial direction vs. distance from tube edge at a displacement of 0,8 mm.	74
6.14	Strain in axial direction vs. distance from tube edge at a displacement of 1,5 mm.	74
6.15	Strain in axial direction vs. distance from tube edge at a displacement of 2,5 mm.	75

6.16	Strain in axial direction vs. distance from tube edge at a displacement of 4,5 mm.	75
6.17	Axial strain in optical fiber and in FEA model at a crosshead displacement of 1,5 mm.	76
6.18	Axial strain in optical fiber and in FEA model at a crosshead displacement of 2,5 mm.	77
6.19	T2 and T3 vs. displacement, plotted with FEA results. . . .	77
6.20	T4, T5 and T6 vs. displacement, plotted with FEA results. .	78
6.21	Percent wise difference between FEA and experimental results.	79

List of Tables

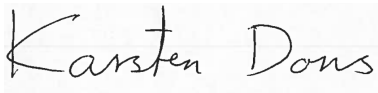
2.1	Design requirements	16
2.2	Material properties for knitted unidirectional Hipertex material obtained by Perillo [5].	18
2.3	Fabric data for Devold DBL 800 E10-H tri-axial fiber mat, stitching etc. excluded.	18
2.4	Material properties used for unidirectional e-glass-epoxy[6]	19
2.5	Material properties for cured Axson UR 3435/3442 [7]	19
2.6	Fiber angle distribution of the selected laminate	28
2.7	Laminate loads	29
2.8	Load proportionality factors for different loads. Listed from tube inside to outside.	30
2.9	Expected failure pressures and axial loads at failure.	31
3.1	Production summary. Letters under section refers to letters in Figure 2.3	41
3.2	Laminate thickness area A	45
3.3	Laminate thickness area E	45
3.4	Fiber distribution of the produced laminate	46
3.5	Bolt hole diameter	46
3.6	Edge distance	46
3.7	Fiber volume fractions	50
3.8	Expected failure pressures and axial loads of the produced laminate.	51
A.1	Sample tube layup as estimated. Inside ply to the bottom.	100
A.2	Sample tube layup as produced. Inside ply to the bottom.	101
A.3	Load propotionality factors for the produced laminate at maximum load obtained during tensile testing.	102
A.4	Load propotionality factors for the produced laminate at the linear limit load found during tensile testing.	103

Preface

The following report is the masters thesis of stud.techn Karsten Dons, written in 2013. This research is the final work in the process of finishing the degree of Master of Science in mechanical engineering at the Norwegian University of Science and Technology. The candidate has been a part of the Composite group at the Department of Engineering Design and Materials.

The author would like to express his gratitude to the people supporting his work. Supervisor Professor Andreas Echtermeyer for valuable discussions and letting the author work with this new end fitting design. It has been great to investigate a new concept and take part in the development of a technology for possible future practical use. PhD student Jon Harald Lambert Grave has been of great help with laboratory work and instrumentation. PhD student Kaspar Lasn for valuable help investigating different bushings and PhD Student Stanislav Schebetov for help with literature search.

The author would also like to thank co-students at room 212 for the wonderful working environment at the office.

A handwritten signature in black ink on a light-colored background. The signature reads "Karsten Dons" in a cursive, slightly slanted script. The letters are connected, and the overall appearance is that of a personal signature.

Trondheim 10.6.2013

Chapter 1

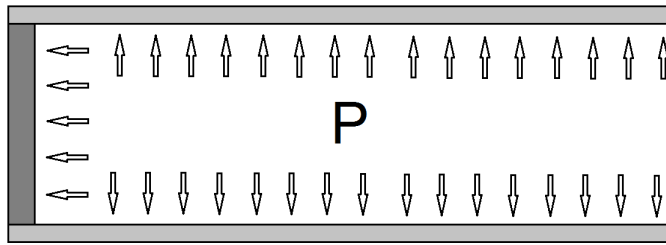
Introduction

1.1 Introduction

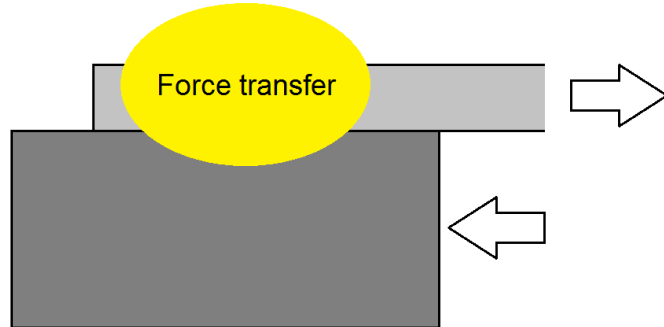
In this thesis a new end fitting design for composite tubes proposed by Professor Echermeier has been investigated.

End fittings is a trouble spot for composite tubes. In some applications it is crucial with a strong connection between the tube and other components and this connection is difficult to design in a simple and strong way. There are several problems related to making an end fitting for composite tubes. It is difficult to distribute the load to all plies in the composite and the different mechanical behavior of composites and metals cause problems.

Composite material has found a wide use where high strength and light weight is needed. The technical difficulties with a metal-composite connection has sometimes caused the weight savings gained by using composites to be lost in the massive reinforcements sometimes needed around the joint [8].



(A) Pressure inside a tube. End fitting in dark grey.



(B) Force transfer in end fitting connection

FIGURE 1.1: End fitting physics

Joints for composite materials can be classified in mechanical joints and adhesive joints. Mechanical joints use mechanical interlocking while adhesive joints use an adhesive to join the parts together. Combinations of a mechanical and adhesive joint can also be used.

Mechanical joints can further be split into bolted and interlocking joints. Bolted joints utilize bolts with threads and nuts while interlocking joints uses other mechanical systems. Pinned joints are a special case of bolted joints where the bolt is replaced with a pin instead.

1.2 End fitting physics

An generic sketch of an tube with internal pressure and an end fitting is seen in Figure 1.1a. The internal pressure is acting on both the end fitting

and the tube.

The pressure acting on the surface of the end fitting can be treated as an axial load on the end. Due to force balance in the end fitting-tube interface there has to be force transfer from the end fitting to the tube as seen in Figure 1.1b. The key concept of an end fitting is to make an efficient and reliable way of transferring the pressure load on the end fitting to the composite tube while keeping the tube end sealed.

End fittings and composite tubes can be used for various applications like drive shafts, beams and struts. The key concept is still load transfer between the end fitting and tube, but the direction and kind of load differs.

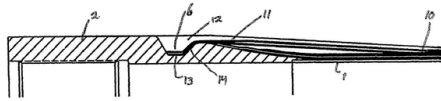
1.3 Previously suggested end fittings

Various end fittings for composite tubes have been designed and patented. The patents presented here are illustrated in Figure 1.2.

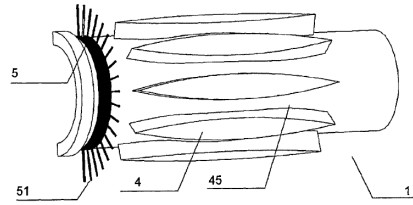
The trap lock designed by Paulshus et al. [9] is one of the well tested designs. The joint utilizes a system of grooves on the end fitting that the wound composites interlock in and thereby creates a mechanical lock [9].

Gustafson and Vedvik [10] proposed an end fitting where the composite material is wound around radial fins on a hub to achieve a wedging effect to mechanically lock the fibers. This is an advanced joint as it requires advanced geometries and a custom made winding program to produce the joint.

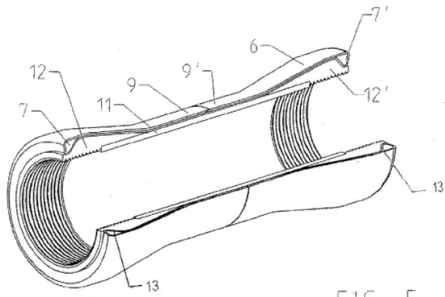
Fahey and Mueller [11] designed an end fitting where axial fibers are wound on a long mandrel with the end fittings inside, at some distance from the ends. Near axial plies are then wound and tied down with hoop fibers in a groove in the end fitting. The fibers are then cut at the end of the mandrel and folded back on to the tube. This design locks all axial fibers in to the end fitting and therefore withstands high axial loads.



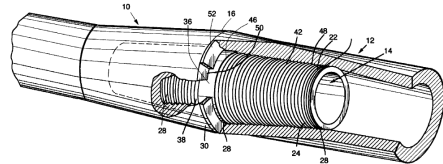
(A) Illustration of patent by Paulshus et al. [9].



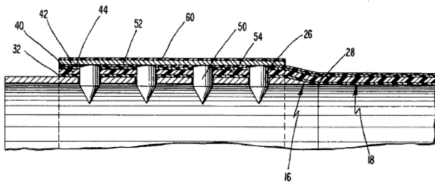
(B) Illustration of patent by Gustafson and Vedvik [10].



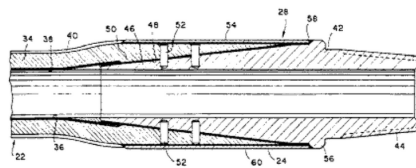
(C) Illustration of patent by Fahey and Mueller [11].



(D) Illustration of patent by Carstensen et al. [12].



(E) Illustration of patent by Yates and Presta [13]



(F) Illustration of patent by Tew [14]

FIGURE 1.2: Patents

Carstensen et al. [12] suggested a joint based on threads. A metal end fitting with conical threads are screwed in to a threaded composite tube. The tube is wound on a mandrel with the desired thread form in the end and the end fitting is screwed in after curing and extraction of the mandrel.

Yates and Presta [13] utilizes a filament wound tube together with radial pins pressed through the wound material while it is uncured. The tube is wound on the outside of a sleeve and then pins are pushed from the outside

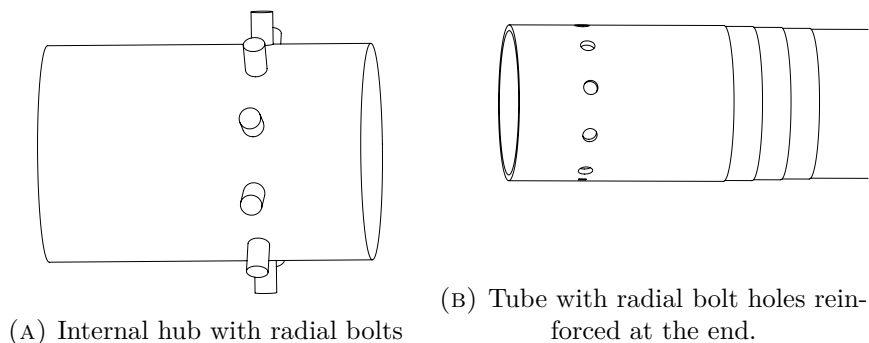


FIGURE 1.3: Idea illustration

through holes in the inside sleeve. The material is then cured and an outer sleeve is added.

Tew [14] designed an end fitting for composite drill pipes. It utilizes a conical hub together with press fit pins to connect the composite to the hub. The composite drill string is made with a conical end where the hub is glued in. Then holes are drilled through the composite and into the hub. Press fit pins are then fitted in the holes.

1.4 New design proposed by Prof. Echtermeyer, NTNU

The new end fitting design consist of two main components: A specially made composite tube and a radially bolted connection.

A new production method is used to optimize the composite tube for the present load in the center and for a bolted connection capable of handling the load in the ends. The desired layup and thickness necessary for a bolted connection is often significantly different from what is necessary to carry the load in a plain laminate. If only a short section around the ends is optimized for a bolted connection and the rest of the tube optimized for

the load, large amounts of material and weight can be saved compared to a pipe with bolt area layup over the whole length. How this is done is further explained in Chapter 2.

The radially bolted connection and the layup can be tailor made to fit the load present. With a custom made end fitting the tube can be versatile and fit various applications such as riser joints, process equipment and possibly drive shafts.

The radially placed bolts are connected to a hub. There are two possible locations for the hub, the inside and outside of the composite tube. A inside hub is illustrated in Figure 1.3a.

This end fitting design might come in conflict with several of the patents mentioned in Section 1.3 and others. None of the investigated patents mentions both the reinforcement of the composite tube, the production method necessary and a radially bolted connection. Patent issues have not been considered in this thesis.

1.5 Introduction to bolted joint geometry

In this section basic nomenclature and simplifications for bolted joints are introduced.

With radial bolts in the end fitting the axial pressure load described in Section 1.2 transforms in to a shear load in bolts as illustrated in Figure 1.4.

Central measures in bolted joint geometry is the bolt diameter, d , and the distance between them, the pitch, p , if there are several bolts. The pitch is the distance from bolt center to the next bolt center transverse to the load direction. The edge distance, e , is the distance from the center of the bolt to the edge of the laminate along the loading direction. The distance from

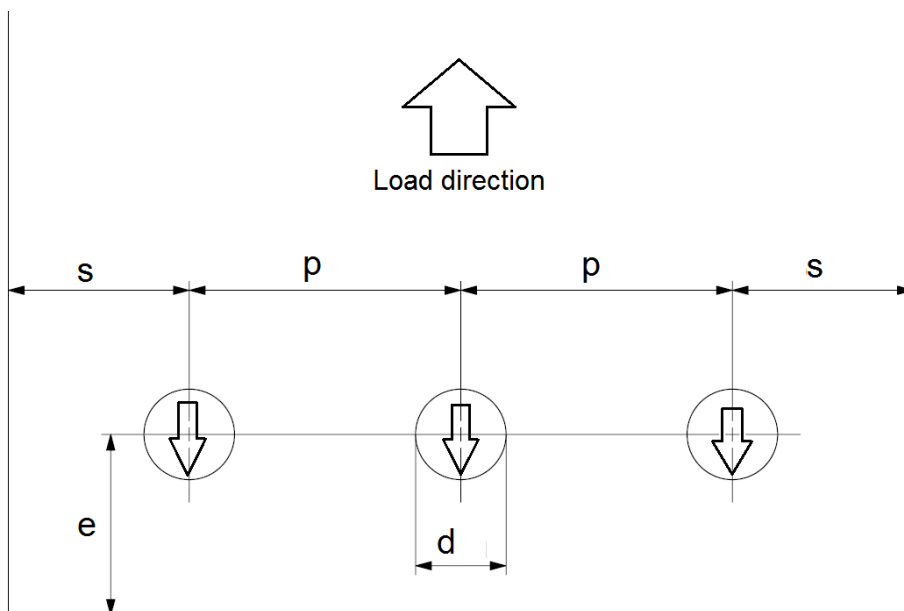


FIGURE 1.4: Joint geometry for a single row joint.

the side edge of the laminate to first bolt center is denoted s . A single row joint is illustrated in Figure 1.4. If the bolted joint has several rows of bolts, the pitch between the rows is known as back pitch.

A joint with multiple bolts is often drawn simplified as in Figure 1.5. The drawing only illustrates one bolt hole and half of the pitch to each side. This simplifies the drawing as only one bolt is handled. If one uses this simplification in calculations, edge effects are ignored.

Radially bolted joints in tubes are somewhat different from flat plate joints. In flat plate joints, edge effects have to be considered, while for circular joints, there are no free edges and the joint can therefore be considered infinitely wide. The simplified drawing in Figure 1.5 is therefore suitable for circular joints in tubes.

Radially bolted joints place some constraints on the joint geometry. The pitch is directly controlled by the number of bolts if the tube diameter is

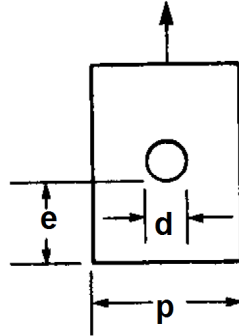


FIGURE 1.5: Simplified drawing of a bolted connection. Figure adapted from Chamis [1].

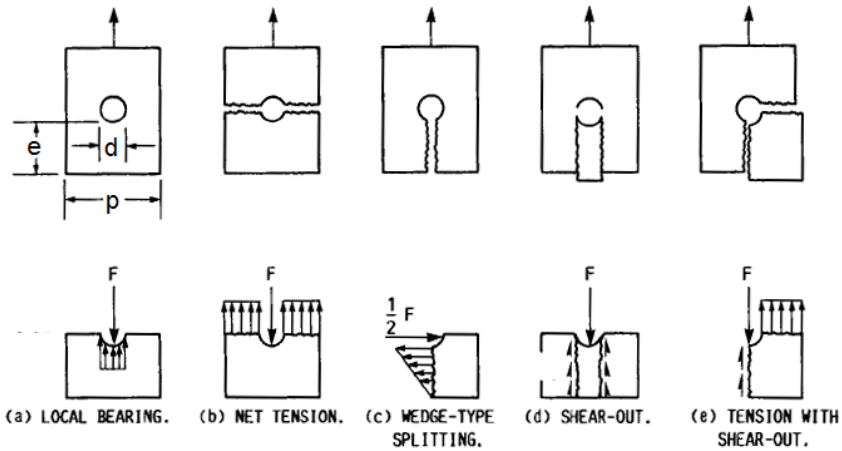


FIGURE 1.6: Failure modes. Figure adapted from Chamis [1].

kept constant. The number of bolts and bolt diameter then becomes an optimization problem when the highest strength possible is wanted.

1.6 Failure modes of bolted joints

The failure modes as presented by Chamis [1] are illustrated in Figure 1.6.

Several failure modes must be considered in composite bolted joints. It is especially important to treat all failure modes when using composites in bolted connections as the laminate properties in different directions might vary a lot from laminate to laminate.

Local bearing failure is failure in compression in the bolt-laminate interface. This is the preferred failure mode as it is not catastrophic [8]. Net section failure is failure in tension in the cross section between the bolts. It occurs when the axial strength in load direction is exceeded in the cross section between the bolts. Wedge-type-splitting is the splitting of the laminate in a cross section between the bolt hole and the edge. It occurs when the strength transverse to the load direction is exceeded. This is a failure mode associated with laminates with little strength transverse to the load direction. Shear-out is failure in shear where the area between the bolt and the edge is pushed out of the laminate. It occurs in laminates that have little shear strength or a short edge distance. Mixed mode failure with net section and shear out is a combination between shear out and net section failure.

1.7 Recommendations for bolted joint geometry

Some of the textbooks about composites mentions bolted joints and presents recommendations. The most important findings are summarized here.

1.7.1 Handbook of composites

Dastin [15] presents several guidelines for bolted connections. A $p/d=5$ is according to Dastin [15] suitable for joints with large safety factors while 4 is a minimum value. For a laminate thicker than 5 mm he suggest a $e/d>2$. Regarding the bolt diameter a conservative d/t is 1 while 3 is generally sufficient.

1.7.2 Composite Design

Tsai [16] presents many useful design charts for bolted joints where several layups and geometries are presented. No specific guidelines on generic measures are presented, but a graph for strength reduction factor for different p/d ratios is presented. For d/t he suggests that a value larger than 1 should be used.

Regarding layups it is stated that laminates containing 50% fibers in load direction achieves the highest bearing strengths, and that the presence of $\pm 45^\circ$ fibers is beneficial for the compressive strength.

1.7.3 Composite airframe structures

Niu [8] presents several recommendations for bolted joints. He suggests $e/d > 3$ and a $p/d > 5$. A quasi isotropic layup is suggested, with a minimum of 40% $\pm 45^\circ$ fibers and 10% of the fibers transverse to the load direction. A graph over stress concentration factors plotted against p/d ratio is presented. It shows an exponential increase in stress concentration factor for decreasing p/d ratio. For a p/d ratio of 2 a stress concentration factor of 5 is suggested. A stress concentration of 3.5 is suggested to use with a $p/d = 3$.

1.7.4 A design methodology for mechanically fastened joints in laminated composite materials

Camanho and Lambert [17] presents a design methodology for bolted joints. It is a thorough description on how to predict the onset of damage, final failure and failure mode in bolted joints. Their method applies the Yamada-Sun failure criterion at a characteristic line, at a specified distance from the hole. This characteristic distance is treated as a material/laminate constant and experiments are needed to determine the distance. Their methodology

is therefore not suitable for early phase design, as a lot of experimental work is needed.

1.7.5 Effect of stacking sequence and clamping force on the bearing strengths of mechanically fastened joints in composite materials

Parker [18] found a relation between the ply stacking sequence and bearing strength. Laminates with 90° fibers on the outside could withstand higher loads before delamination compared to other configurations.

1.8 Applicable standards

The author has not been able to find any design standards describing the detailed design of bolted joints in composite materials. DNV Offshore standard DNV-OS-C501 "Composite components" is a design standard for composite components used offshore, but the standard is not specifying any detailed design requirements [19]. In section 7 B111 it say: "The most practical approach is likely to use a combination of analysis and testing."

Although there are no standards for detailed design there are standards for testing of specimens with open or filled holes, bearing strength and pull through strength [20–23]. ASTM D953-10: "Standard test method for bearing strength of plastics", defines the bearing strength as the load at a hole elongation of 4% while ASTM D5961/D5961M-10: "Standard test method for bearing response of polymer matrix composite laminates", operates with a bearing offset strength at 2% hole elongation, and ultimate strength at the maximum bolt load.

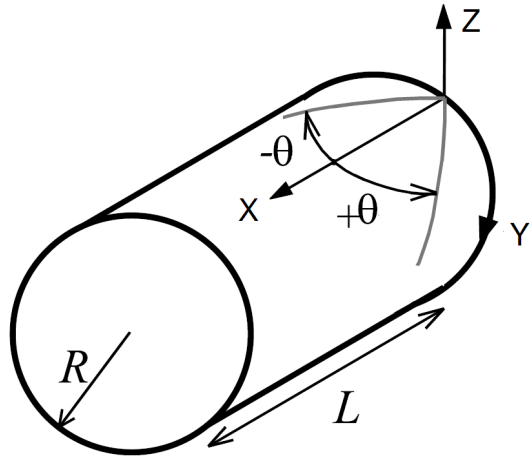


FIGURE 1.7: Winding angle Θ . Figure adapted from Messenger et al. [2].

1.9 Winding or fiber angle definition

In filament winding the winding angle is defined as the angle the strand or fiber has against an imaginary axis going in the axial direction on the outer surface of the tube, as illustrated in Figure 1.7. Wherever fiber orientation is used in this thesis, it follows this definition, both for wound material and stitched mats. Following this definition of a coordinate system the load direction as defined in Figure 1.4 for the radial bolts will always be along the X-axis as illustrated in Figure 1.7.

1.10 Laminate theory

Laminate theory is a good way of establishing a load-deformation relation for a composite laminate. The full explanation of laminate theory is not treated here. Textbooks like Kollar and Springer [24] and Vedvik [25] give a thorough explanation. Wherever laminate theory is used in this thesis the axis is defined as in Section 1.9 having the X-axis of the laminate in axial direction and Y in hoop direction.

The framework of laminate theory is based on the following assumptions [25]:

- Plane stress state.
- Strains vary linearly through the thickness.
- Displacements are small compared to the thickness of the laminate.
- Out-of-plane normal strains and shear strains are neglected.
- Normal distance from any point to the middle surface remains constant.
- The laminate is considered infinitely wide.

A load deformation relation for a laminate is established based on these assumptions. The load deformation relation is stated in Equation 1.1.

$$\begin{bmatrix} N_x \\ N_y \\ N_{xy} \\ M_x \\ M_y \\ M_{xy} \end{bmatrix} = \begin{bmatrix} A_{xx} & A_{xy} & A_{xs} & B_{xx} & B_{xy} & B_{xs} \\ A_{xy} & A_{yy} & A_{ys} & B_{xy} & B_{yy} & B_{ys} \\ A_{xs} & A_{ys} & A_{ss} & B_{xs} & B_{ys} & B_{ss} \\ B_{xx} & B_{xy} & B_{xs} & D_{xx} & D_{xy} & D_{xs} \\ B_{xy} & B_{yy} & B_{ys} & D_{xy} & D_{yy} & D_{ys} \\ B_{xs} & B_{ys} & B_{ss} & D_{xs} & D_{ys} & D_{ss} \end{bmatrix} \begin{bmatrix} \epsilon_x^0 \\ \epsilon_y^0 \\ \epsilon_{xy}^0 \\ \kappa_x \\ \kappa_y \\ \kappa_{xy} \end{bmatrix} \quad (1.1)$$

In Equation 1.1, N_i and M_i are in plane load and moment per length unit and A_{ij} is the in plane stiffness matrix. B_{ij} is the in-plane out-of-plane coupling matrix and the D_{ij} the bend-twist coupling matrix. ϵ_{ij}^0 is the mid-plane strains and κ_{ij} is the curvature and twist of the laminate. Laminate loads can then be applied to the laminate as load per length unit and the in plane strain and curvature of the laminate found. The laminate deformation can then be back calculated to stresses and strains in the individual plies.

1.10.1 Maximum stress criterion

The maximum stress criterion was used to determine the onset of ply failure and failure mode of the plies. The maximum stress criterion can be written using a load proportionality factor, f , as stated in Equation 1.2 for a plane stress state.

$$f = \max\left(\frac{\sigma_1}{X_T}, \frac{-\sigma_1}{X_C}, \frac{\sigma_2}{Y_T}, \frac{-\sigma_2}{Y_C}, \frac{-\tau_{12}}{S_{XY}}\right) \quad (1.2)$$

Where σ_1 and σ_2 is the stress in parallel and transverse to the fiber. τ_{12} is the in plane shear. When f is greater than unity the load exceeds the strength and the ply fails. The different terms in Equation 1.2 corresponds to different failure modes of a ply, fiber failure in tension, fiber failure in compression, matrix cracking or matrix failure in tension, matrix crushing or matrix failure in compression, and shear failure.

Chapter 2

End fitting design

A sample tube has been designed to verify the end fitting idea by Professor Echtermeyer as described in Section 1.4. Design requirements and constraints have been found and a suitable end fitting has been optimized and dimensioned.

2.1 Design requirements and limitations for the sample tube

In order to make a sample tube to verify the idea illustrated in Section 1.4 some design requirements had to be established. The design was limited by engineering judgment, safety requirements and practical limitations.

A failure pressure of 20 MPa or 200 bar was selected.

A mandrel for making a tube with an inner diameter of 100 mm was readily available in the lab and to avoid the expense of making a new mandrel it was decided to use this mandrel. This limits the design to a tube with inner diameter 100 mm.

TABLE 2.1: Design requirements

What	Value
Design/Failure pressure	20 MPa
Axial load at failure	157 kN
Internal diameter	100 mm
Materials	Hipertex filament winding material Devold DBL 800 E10-H triaxial e-glass Axson UR 3435/3442 casting polyurethane

Different fiberglass materials were available in the lab. Hipertex filament wound fiberglass [26] and e-glass fibers in Devold DBL 800 E10-H tri-axial mats [27] were used. Both with Momentive Epicote epoxy resin [28]. Axson UR 3435/3442 [7] casting polyurethane was obtained to make an internal liner.

The design requirements are summarized in Table 2.1. The axial load was found using Equation 2.1 where F_{axial} is the axial force, D_i is the inner diameter of the tube and P is the pressure [29]. A failure pressure of 20Mpa and an inner diameter of 100 mm gives an axial force of 157 kN.

$$F_{Axial} = \frac{\pi}{4} D_i^2 P \quad (2.1)$$

2.2 Hub design

An internal hub was selected for the end fitting. As the outer diameter of the tube is unknown before a tube is produced, it seemed favorable to use an internal hub as the hub could be produced before the tube was finished. The hub was designed with an inlet/outlet hole in the center and the bolts placed 50 mm from the inside edge and 100 mm from the outside edge. The choice of having the bolt row 50 mm from the inside edge was taken to avoid having pressure loads near the bolt row and thereby have only an axial load in the area near the bolts. The hub was made out of construction

steel and massively over dimensioned so it could be treated as infinitely stiff and have a large safety factor against failure. In a later production phase, a more optimized hub could be used. The number of bolts and bolt diameter is treated in Section 2.6. A machine drawing of the hub can be seen in Appendix B.

2.2.1 Sealing

Making a composite pipe pressure thigh is not easy. It was outside the scope of this project to find a solution for a good liner system. Main emphasis has been on selecting a simple approach.

Matrix cracking during pressurization of a composite tube lead to leakage unless a liner is used. The liner ensures that the internal liquid (or gas) do not leak out when matrix cracking occurs. It was decided to use a very low viscosity (before curing) two-component polyurethane, Axson UR 3435/3442, as a liner and as a seal between the hub and tube. Liquid polyurethane is applied between the hub and the tube during assembly and an internal liner is added using rotational molding after the hubs are fitted. It has been filed a patent application for this process of applying a liner by PU Teknikk AS [30].

2.3 Material properties

It is difficult to obtain material properties from filament wound components, as it is nearly impossible to make flat samples. Material properties for Hipertex and Epicote epoxy, have been obtained by Perillo [5] for a knitted fiber laminate made with vacuum assisted resin injection, VARI. The material data obtained are listed in Table 2.2. The knitted material had a

TABLE 2.2: Material properties for knitted unidirectional Hipertex material obtained by Perillo [5].

Engineering constant	VARI	Scaled properties
V_f	54%	61,6 %
E_1	44870 MPa	51185,04 MPa
$E_2 = E_3$	12130 MPa	
$G_{12} = G_{13} = G_{23}$	3280 MPa	
$\nu_{12} = \nu_{13}$	0,3	
ν_{23}	0,5	
X_T	1006,30 MPa	1147,93 MPa
X_C	486,00 MPa	554,40 MPa
$Y_T = Z_T$	45,95 MPa	
$Y_C = Z_C$	131,90 MPa	
S_{XY}	49,51 MPa	

TABLE 2.3: Fabric data for Devold DBL 800 E10-H tri-axial fiber mat, stitching etc. excluded.

Orientation	Fiber	Filament diameter	Area Weight
0°	E-glass	14 μ m	414g/m ²
+45°	E-glass	13 μ m	198g/m ²
-45°	E-glass	13 μ m	198g/m ²

fiber volume fraction, V_f , of 54%. ν_{23} was assumed 0,5 and tensile properties in 2 and 3 direction assumed equal. Shear stiffness, G, was assumed equal in all planes.

Fabric data for the Devold fabric is listed in Table 2.3. Material properties for Devold DBL 800 E10-H [27] have not been obtained. Textbook values from Daniel et al. [6] for a unidirectional e-glass epoxy laminate was used and the material data are listed in Table 2.4.

Axson UR 3435/3442 Casting Polyurethane was used as a inside liner. It was selected due to its low viscosity before curing. Material properties for the cured polyurethane are listed in Table 2.5.

Properties listed as "Scaled" are material properties scaled for the fiber volume fraction of the produced pipe as described in Chapter 3.

TABLE 2.4: Material properties used for unidirectional e-glass-epoxy[6]

Engineering constant	Textbook	Scaled
V_f	55%	56,6 %
E_1	41000 MPa	42192 MPa
$E_2 = E_3$	10400 MPa	
$G_{12} = G_{13}$	4300 MPa	
G_{23}	3500 MPa	
$\nu_{12} = \nu_{13}$	0,28	
ν_{23}	0,50	
X_T	1140 MPa	1173,17 MPa
X_C	620 MPa	638,04 MPa
$Y_T = Z_T$	39 MPa	
$Y_C = Z_C$	128 MPa	
S_{XY}	89MPa	

TABLE 2.5: Material properties for cured Axson UR 3435/3442 [7]

Engineering constant	
Hardness Shore A1	65
Tensile Strenght	2,5 MPa
Elongation at break	850 %

2.4 Middle section layup

The middle section of the tube was designed by the formulas for stresses in thin-walled cylinders [31]. The two equations for hoop and axial stress, σ_{hoop} and σ_{axial} , as a function of wall thickness t , radius R and pressure P for a thin walled cylinder are stated in Equation 2.2 and 2.3.

$$\sigma_{hoop} = \frac{R}{t} \cdot P \quad (2.2)$$

$$\sigma_{axial} = \frac{R}{2t} \cdot P \quad (2.3)$$

Using netting analysis as described by Roylance [32], complete matrix cracking is assumed and load is supported in fiber direction only. Any additional

strength added by the liner was ignored as the liner is very soft compared to the composite. If the layup is optimized with these equations, the result is a laminate that is two times stronger in hoop than in the axial direction. The most common layup to use for internal pressure pipes is the $[\pm 55^\circ]$ layup, as it is favorable for the production time for long pipes.

A different approach is to start with a $[0_n^\circ/90_n^\circ]$ type laminate and assume that all the stress in axial direction are supported by the axial plies and the tension in hoop direction supported by the hoop plies. In production, the fiber angle will diverge slightly from 0 and 90, to approximately $12,7^\circ$ and 89° degrees. This leads to a reduction in strength in hoop and axial direction that is less than 3% and therefore ignored. σ_{hoop} and σ_{axial} were replaced by $X_T = 1006,0$ MPa for Hipertex [5] in Equation 2.2 and 2.3 and the necessary thicknesses calculated. From experience a ply thickness of 0,3 mm was assumed and a minimum number of plies obtained. Two plies with axial fibers and four plies of hoop fibers were necessary to carry the load. This number of plies results in an expected burst pressure of 20,6 MPa.

A $[0_n^\circ/90_n^\circ]$ type laminate was selected for the test tube as it is a better layup than $[\pm 55^\circ]$ in the bolted area. Axial loads have to be transferred from the bolt area to the middle of the pipe and axial fibers are therefore favorable.

2.5 Load distribution

The bolt load was obtained by dividing the axial force found in Equation 2.1 with the number of bolts. This leads to Equation 2.4.

$$F_{bolt} = \frac{\pi}{4} D_i^2 \frac{P}{N} \quad (2.4)$$

D_i is the inner diameter of the tube, P is the pressure and N is the number of bolts in Equation 2.4. A failure pressure of 20 MPa and a D_i of 100mm, as

stated in Table 2.1, lead to a bolt force of 15,7 kN per bolt. Due to the lack of better methods, laminate theory was used to determine the p/d ratio and investigate the selected laminate. Laminate theory as explained in Section 1.10 together with the maximum stress criterion described in Section 1.10.1 was used.

2.5.1 Bearing load

Two different approximations were used when calculating the bearing load. The simplest is to assume constant load over the bolt face. It can be argued that during the onset of matrix cracking and failure, small parts of the laminate will yield and the load will be distributed evenly over the bolt face. The equation for a constant load is stated in Equation 2.5. This is the same distribution as used by Chamis [1].

$$N_x = \frac{F_{bolt}}{d} \quad (2.5)$$

N_x is the distributed load in N/mm and d is the bolt diameter. The more conservative assumption is a cosine distribution over the bolt face. Ingvar Eriksson [33] found that the load distribution was indeed not cosine distributed but it is a simple approximation giving a more conservative result than a constant distribution. The maximum load with a cosine distribution was found by Equation 2.6.

$$N_x = \frac{\pi}{2d} F_{bolt} \quad (2.6)$$

N_x is the maximum load in N/mm at the center of the bolt.

2.5.2 Net section load

The net section load was found using Equation 2.7.

$$N_x = \frac{F_{bolt}}{p - d} K_t \quad (2.7)$$

K_t is a stress concentration factor. Niu [8] refers to a diagram from Hart-Smith [34] for suggested stress concentration factors for bolt holes with different e/d and p/d ratios. In his work, he suggests a stress concentration factor between three and four for the p/d ranges applicable here.

2.5.3 Shear out load

The shear out load was found using Equation 2.8

$$N_{xy} = \frac{F_{bolt}}{e} \quad (2.8)$$

Where e is the edge distance and N_{xy} is the shear load. This is the same distribution as used by Chamis [1].

2.5.4 Wedge splitting load

The wedge splitting load was assumed to be linearly distributed between a maximum load at the bolt face and no load at the tube edge. This is the same distribution as used by Chamis [1].

$$N_y = \frac{1}{e - \frac{1}{2}d} F_{bolt} \quad (2.9)$$

N_y is the maximum load in N/mm at the bolt face.

2.5.5 Combined failure

Combined failure is a combination failure including wedge splitting and net section failure. Combined failure has not been treated here because an over-dimensioned edge distance has been used. An edge distance that is over-dimensioned makes this failure mode very unlikely. This is explained in Section 2.7.

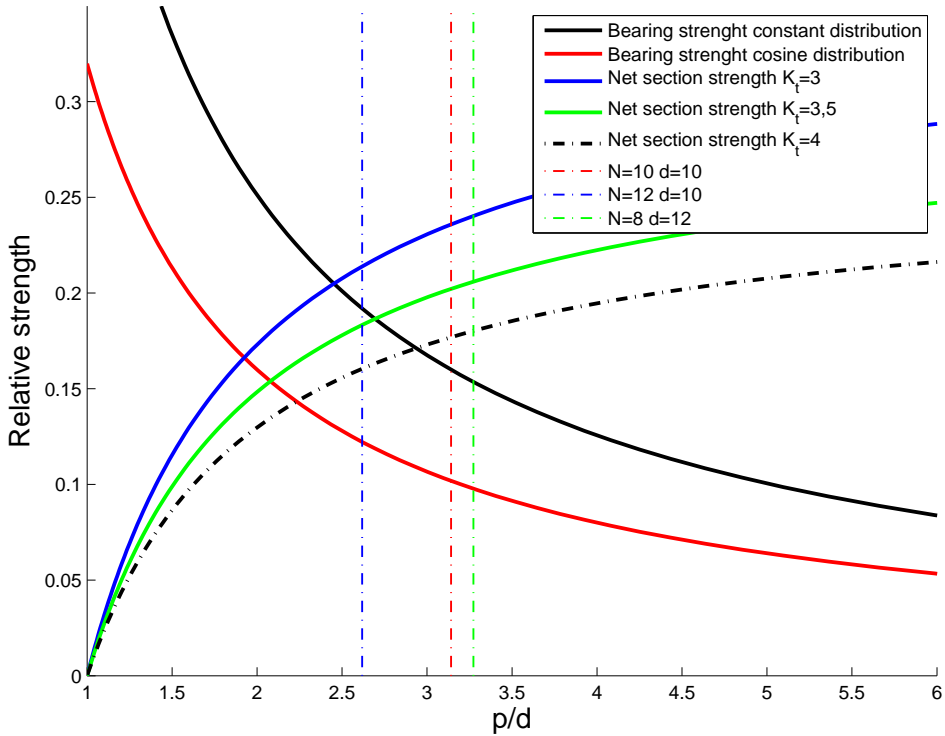
2.6 Number of bolts and bolt diameter

The number of bolts and bolt hole diameter is a tradeoff between net section failure and bearing failure. Too many bolts will give net section failure and too few will give bearing failure before the maximum capacity of the joint is exploited. Pitch and bolt diameter only affects the net section and bearing failure, no other failure modes have to be considered when optimizing the p/d ratio.

p/d ratio is a function of number of bolts and bolt diameter when the tube diameter is kept constant. It follows the relation stated in Equation 2.10 where N is the number of bolts d is the bolt hole diameter and D is the diameter of the tube. With a constant tube diameter, the p/d ratio is a function of N and d.

$$p/d = \frac{Nd}{D\pi} \quad (2.10)$$

In order to simplify the optimization it was decided to look at the relative strength difference between net section strength and bearing strength of a unidirectional laminate. Applying Equation 2.5 to 2.7 makes it clear that it is the laminate strength in load direction (X), that is the limiting factor. If one is to follow Dastin [15] recommendations of 50% 0° fibers, the strength

FIGURE 2.1: Relative failure strength vs. p/d .

of the 0° plies is the most important strength contributor in bearing and net tension failure. All other plies were therefore neglected.

In Figure 2.1 a normalized failure load for net section and bearing failure with a laminate containing only 0° fibers is plotted towards p/d ratio, together with vertical lines representing different bolt combinations. Load distribution from Equation 2.5 to 2.7 was used with material data for Hipertex from Table 2.2. The net section strength is plotted with a stress concentration factor of 3, 3,5, and 4. The maximum stress criterion as described in Section 1.10.1 was used to determine the failure load.

In a bolted joint bearing failure is the preferred failure mode as it has rest strength after initial failure while net section failure is sudden and catastrophic [1]. Looking at Figure 2.1 a safe p/d ratio is then in the area

where the net section strength is larger than the bearing strength. Taking a worst case scenario with $K_t = 4$ and a cosine distribution of the bolt load p/d should then be greater than 2,9.

Different combinations of bolt diameter and number of bolts for a tube with diameter 100 mm are plotted in Figure 2.1 using Equation 2.10. 10 bolts with a diameter of 10 mm gives a p/d ratio of 3,14 and it is the combination that is closest, on the safe side using standard metric bolt dimensions. 10 bolts with 10 mm diameter were therefore used.

The selected p/d ratio of 3,14 is smaller than the p/d ratios suggested by the books, investigated in Section 1.7. p/d ratios in the range from 4 to 5 is recommended.

2.7 Edge distance

The edge distance affects both shear out, wedge splitting and the combined failure mode as seen from Equation 2.8 and 2.9. In the end fitting design the edge distance is the measure in is easiest to increase without side effects. Increasing the edge distance only affects the length of the hub. In this early desing stage a longer hub is not affecting the performance of the end fitting.

It was decided to use a large edge distance to have a large safety factor against shear out, wedge splitting and the combined failure mode. It is from a research point of view more interesting to have a bearing or net section failure to check if the relatively small p/d ratio is sufficient. It was therefore decided to use a e/d ratio of 5. 10 mm bolt holes gives an edge distance of 50 mm. The selected e/d ratio of 5 is large compared to the e/d ratios suggested by the books investigated in Section 1.7 where e/d ratios of 2-3 were suggested.

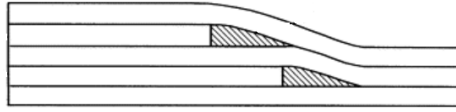


FIGURE 2.2: Ply drop off. Adapted from Mukherjee and Varughese [3]

2.8 Transition area

A limitation to filament winding is the ability to wind components with varying diameter and sharp transitions. The edge of a added mat is a sharp transition as the diameter suddenly decreases or increases with two mat thicknesses. This leads to the phenomena known as bridging [35]. The fiber strand leaves the surface of the previous ply and "shortcuts" before it again lands on the surface as illustrated in Figure 2.2. If the transition is smooth and the winding angle altered this bridging can be avoided. With the added mats, this instant change in diameter is inevitable too sharp and cannot be avoided. A helical ply wound over a mat edge will bridge.

To minimize the stress concentration made by this gap one should fill the gap, illustrated by the shaded area in Figure 2.2, with something that might decrease the stress concentration. The relatively thin added mats makes it difficult to use core material or short fiber mass in the gap. It was therefore decided to rely on excess epoxy squeezed out of the mats to fill the gap and reduce the stress concentration.

2.9 Bolt area layup

The bolt area layup has various practical aspects and recommendations to accommodate if it is to follow the recommendations found in the literature.

- The helical wound plies have to be next to each other. This is an effect of the winding process as the axial plies is wound back and forth

while the mandrel is rotating the same way. This creates a pattern where $+12, 7^\circ$ and $-12, 7^\circ$ fibers are interwoven in a pattern that can be considered random. These two plies are therefore treated as two $\pm 12, 7^\circ$ plies.

- Parker [18] found a relation between the outer ply orientation and bearing strength. He found that 90° fibers in the outer plies is favorable for the elastic load limit of a pinned joint. It is therefore favorable to have 90° plies at the inside and outside of the tube.
- The added mats need to transfer the axial load from the bolts to the pure wound material in the center part. The load is transferred through interlaminar shear between the plies. If the interlaminar shear strength is exceeded, it appears as delamination in the interface between the plies. Any weakness or material flaws in the interface increases the chance of delamination in the interface. It is therefore a good idea to minimize the number of plies between the helical wound plies and 0° plies in the mats. The two wound helical plies should therefore have two 0° plies next to them.
- As explained in Section 2.8, winding a helical ply over a added mat creates a gap in the laminate. This implies that the helical plies should be on the very inside of the tube, alternatively the number of mat edges the axial wound layers have to pass over should be minimized.
- Hoop plies towards the outside of the laminate is favorable for the volume fraction as the hoop plies adds compressive forces to the plies underneath [36]. This compression increases the fiber volume fraction of the plies.
- It has long been agreed that quazi-isotropic laminates are the best layup for bolted joints [8]. Niu [8] suggest a quazi isotropic layup with 40% $\pm 45^\circ$ fibers. There are very few wound axial fibers so to get close to 50% 0° as recommended by Tsai [16], and 40% $\pm 45^\circ$, plies with $\pm 45^\circ$

TABLE 2.6: Fiber angle distribution of the selected laminate

Orientation	Fraction	Recommended fraction
0° and $\pm 12, 7^\circ$	45,6%	50%
$\pm 45^\circ$	33,7%	40%
90°	20,7%	10%

and 0° fibers have to be added. Triaxial mats such as Devold DBL 800 E10-H is suitable.

- Having the added mats going over another mats edge is impossible without altering the fiber angle and possibly generating a gap as described in Section 2.8. It was therefore decided that the innermost mat should be the one that is extended furthest from the tube end and the mats are cut successively shorter going towards the outside of the tube as illustrated in Figure 2.2.
- It is favorable for the production process described in Chapter 3 to add as few mats as possible before a new wound ply is added. The mats may not stick well to the mandrel and possibly get misaligned during application.
- The mats that are added have to be handled before they are placed on the mandrel. Mats that are dimensionally stable while being handled is therefore favorable.

With all these guidelines it was decided to use one layer of Devold DBL 800 E10-H triaxial knitted mat in between the wound plies. A thickness of 1 mm was assumed for the mat. The selected laminate for the bolt area listed under section E in Table A.1.

Using the laminate listed in Table A.1 will lead to a distribution between the fiber angles as listed in Table 2.6. As seen from table 2.6 the laminate do not meet the recommendations of Niu [8] and Tsai [16] but it is less than 11 percentage points from the recommended values.

TABLE 2.7: Laminate loads

Bolt Force	$F_{Bolt} = 15.7 \text{ kN}$
Bearing load constant distribution	$N_x = -1570,8 \text{ N/mm}$
Bearing load cosine distribution	$N_x = -2467,4 \text{ N/mm}$
Net section load $K_t = 4$	$N_x = 2933,9 \text{ N/mm}$
Net section load $K_t = 4$	$N_x = 2200,4 \text{ N/mm}$
Shear out load	$N_{xy} = 261,8 \text{ N/mm}$
Wedge splitting load	$N_y = 628,3 \text{ N/mm}$

2.10 Laminate theory

To investigate the selected layup further laminate theory was used in lack of better models that are sufficiently simple.

Laminate theory as described in Section 1.10, together with the maximum stress criterion described in Section 1.10.1 were implemented in a spreadsheet. Material data as listed in Section 2.3 was used together with the load distributions described in Section 2.5. The laminate in the bolt area is listed in under E in Table A.1.

The loads were calculated using Equation 2.4 to Equation 2.9 and listed in Table 2.7. The calculated loads were entered in the spreadsheet and the corresponding load proportionality factor was logged for each ply. The load proportionality factors are listed in Table 2.8.

TABLE 2.8: Load proportionality factors for different loads. Listed from tube inside to outside.

Ply nr	Angle [deg]	Bearing load constant		Bearing load cosine		Net section $K_t = 4$		Net section $K_t = 3$		Shear out		Wedge splitting	
		f	Exceeded	f	Exceeded	f	Exceeded	f	Exceeded	f	Exceeded	f	Exceeded
1	90	0,74		1,16	Y_C	3,97	Y_T	2,97	Y_T	0,29		0,16	
2	-45	0,56		0,88		2,00	Y_T, S_{XY}	1,50	Y_T, S_{XY}	0,42		0,50	
3	45	0,57		0,90		1,99	Y_T, S_{XY}	1,49	Y_T, S_{XY}	0,12		0,47	
4	0	0,62		0,97		0,63		0,47		0,20		0,87	
5	12,7	0,83		1,31	X_C	0,75		0,56		0,26		0,80	
6	-12,7	0,85		1,33	X_C	0,76		0,57		0,25		0,80	
7	0	0,67		1,05	X_C	0,68		0,51		0,20		0,83	
8	-45	0,64		1,00	S_{XY}	2,39	Y_T, S_{XY}	1,79	Y_T, S_{XY}	0,40		0,44	
9	45	0,65		1,01	S_{XY}	2,44	Y_T, S_{XY}	1,83	Y_T, S_{XY}	0,12		0,43	
10	90	0,92		1,44	Y_C	4,92	Y_T	3,69	Y_T	0,28		0,14	
11	0	0,72		1,14	X_C	0,74		0,55		0,19		0,78	
12	-45	0,68		1,07	S_{XY}	2,62	Y_T, S_{XY}	1,97	Y_T, S_{XY}	0,39		0,40	
13	45	0,69		1,09	S_{XY}	2,71	Y_T, S_{XY}	2,04	Y_T, S_{XY}	0,12		0,40	
14	90	1,00		1,57	Y_C	5,35	Y_T	4,01	Y_T	0,27		0,13	
15	0	0,78		1,23	X_C	0,80		0,60		0,19		0,73	
16	-45	0,73		1,14	S_{XY}	2,86	Y_T, S_{XY}	2,14	Y_T, S_{XY}	0,37		0,36	
17	45	0,74		1,16	S_{XY}	2,99	Y_T, S_{XY}	2,24	Y_T, S_{XY}	0,12		0,37	
18	90	1,08	Y_C	1,69	Y_C	5,78	Y_T	4,33	Y_T	0,26		0,12	

TABLE 2.9: Expected failure pressures and axial loads at failure.

	Cosine bearing load and $K_T = 4$		Constant bearing load and $K_T = 3$		Location
	Pressure [Mpa]	Axial load [kN]	Pressure [Mpa]	Axial load [kN]	
Y_T	3	23	5	39	Net-section
Y_C	12	94	19	149	Bearing
S_{XY}	15	118	19	149	Net section
X_C	15	118	24	188	Bearing
X_T	25	196	33	259	Net-Section

The load proportionality factors listed in Table 2.8 were used to determine failure pressures using Equation 2.11. The pressures for first failure for each material failure mode are listed in Table 2.11. Any pressure can be used as P_{Design} in Equation 2.11 as long as it is the same pressure used to find the load proportionality factors since it is a linear relation between pressure, laminate load and load proportionality factors.

$$P_{fail} = \frac{P_{Design}}{f} = \frac{20\text{MPa}}{f} \quad (2.11)$$

As we see from Table 2.9, the first signs of failure is expected to be seen as matrix cracking in the net section at a very low pressure. Matrix cracking and matrix crushing generally occurs at low loads but do not lead to a collapse of the whole laminate. Shear failure is expected to start at a pressure of 15 MPa for a conservative estimate and at 19 MPa for less conservative estimate. Compressive fiber failure is expected to happen in front of the bolt at a pressure of 15 Mpa using a cosine bearing load distribution. Following the assumptions made in Section 2.5 the laminate should fail locally in front of the bolts and the load distribution approach a constant distribution. With a constant distribution, compressive fiber failure is expected to occur at 24 Mpa. Tensile fiber failure is expected to happen at even higher pressures in the net section.

From this, it is expected that the area in front of the bolts will have local damage at 15 MPa and fail completely around 24 MPa.

It is seen from Table 2.9 that bearing failure is very likely to happen before net section failure, as intended. As described in Section 2.6, bearing failure should happen before net section failure using a conservative net section stress concentration and a non-conservative bearing strength.

These estimates are non-conservative, as any damage to the plies are not taken into account. Load bearing in all plies are assumed even after their failure. The sequence of ply failure is likely to be correct but the strength of the laminate might be over estimated as damage is not modeled. Damage modeling is not in the scope of this thesis.

2.11 Sample tube geometry and stagger distance

The lathe available for the liner production limited the maximum length of the sample tube. It was limited to 1000 mm including the end fittings. Using the end fitting described in Section 2.2 results in a composite tube that is 900 mm long including the edge distance of 50 mm.

The added mats had an estimated thickness of 1 mm. A stagger distance of 20 times the ply thickness of the dropped ply was used. A 1:20 relation gives 20 mm between the mat edges and a 60 mm long transition zone with four mats. It was decided to start the transition 50 mm from the edge of the hub to avoid interference between the bolt loads, the edge of the hub and the transition. This places the beginning of the transition 150 mm from the ends of the sample tube after cutting.

The mandrel used has a cylindrical length of 2000 mm. It was decided to use the middle part for the pressure test and make two transition towards the ends for visual inspection specimens and burn off tests. The measurements

of the sample tube is shown in Figure 2.3. The tube for pressure testing was the middle 900mm of the produced pipe.

Letters A to E in Figure 2.3 refers to the layup specified in Table A.1, where the layup is specified for the whole tube is specified.

2.12 Bushings and bolt shear

It was decided to use bushings in the bolt holes. Bushings are used to improve the load distribution. By using a sufficiently soft bushing material any surface roughness in the bolt hole lead to local yielding in the bushing and thereby distribute the load more evenly. The bushing is therefore made out of a softer material than the bolt.

PhD student Kaspar Lasn and the author conducted a short test program with three different bushings. A composite bushing from SKF # CM 081010 E, a plastic bushing from Igus #iglide®J JSM-0810-12 and a copper bushing made out of a copper tube were compared. All the bushings had an inner diameter of 8 mm and an outer diameter of 10 mm.

The bushings were cut in half and placed in a ram and die test setup re-assembling half of a bolt hole as seen in Figure 2.4. The setup was placed in a test machine and the force-displacement curve for the different bushings was obtained.

It can be concluded from the test results that the plastic bushings were too soft to use in this application. They had signs of global yielding at a load lower than the design load for this application. The composite bushings and the copper bushings had almost the same global yield limit. The composite bushings were compliant at a low load before their stiffness increased. This is seen as beneficial as the bushing yields as intended to distribute the load before the stiffness increase. No material data was supplied with the

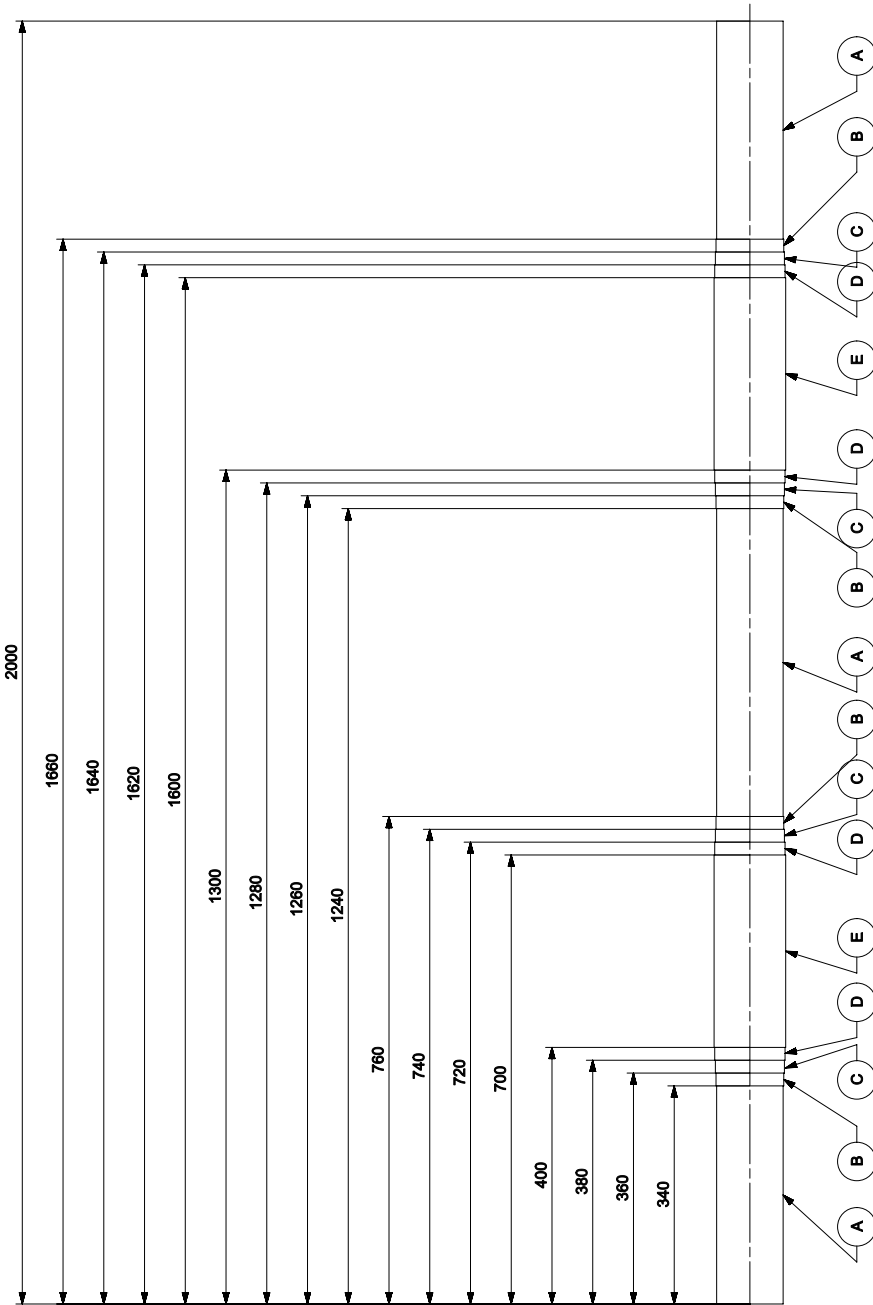


FIGURE 2.3: Tube geomerty, as made on mandel.

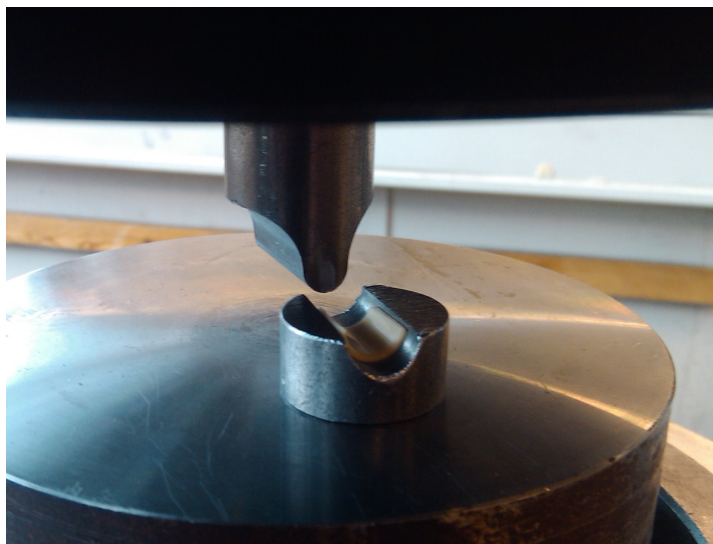


FIGURE 2.4: Bushing test setup. Photo by Kaspar Lasn.

copper tube, so because of repeatability and its favorable properties the SKF composite bushings # CM 081010 E were used.

$$\tau = \frac{F_{bolt}}{A} \quad (2.12)$$

$$\tau = \sigma_y \text{ at yield} \quad (2.13)$$

The use of bushings with $d_i = 8$ mm limits the bolt diameter to 8 mm. The current hub design loads all the bolts in single shear at the hub surface. Using Equation 2.4 together with Equation 2.12 gives the shear stress in the bolt. In Equation 2.12 the bolt cross sectional area is A , which for M8 bolts is $36,6 \text{ mm}^2$. This results in an average shear stress of 429 MPa at a pressure of 20 MPa. The Tresca criterion for yield [31] is stated in Equation 2.13 where σ_y is the yield stress. M8 bolts of 12.9 quality has a yield strength of 1080 MPa giving a safety factor of 2.5 when using the Tresca yield criterion. The safety factor is considered sufficient.

2.13 Limitations

The design of the end fitting impose some limitations on the maximum pressure it is possible to achieve. It is possible to increase the edge distance and laminate thickness but impossible to increase the width of the joint for one tube diameter. One can always increase the laminate thickness and achieve a higher strength in the laminate, only to see the bolts fail instead.

Steel pins with a diameter of 10 mm with a yield strength of 640 MPa can only handle a bolt load of 50,3 kN each without failing in shear. By using Equation 2.4 with $N=10$ and $ID=100\text{mm}$ one finds the theoretical maximum pressure limited by the bolts to be 64 MPa or 640 bar for the current bolt configuration. It is possible to add one or more rows of bolts but this has not been explored further.

Dastin [15] and Tsai [16] suggest to use a $d/t > 1$. In order to have a laminate strong enough to support the maximum load constrained by the bolt strength the laminate would have to be thick and give a d/t value a smaller than 1.

Chapter 3

Tube and end fitting production

A new production method combining wound fibers and stitched mats has been developed. The middle section of the pipe consists of pure wound material optimized for internal pressure while at the ends stitched mats are added to optimize for a bolted connection as described in Chapter 2. First, a short presentation of the filament winding method, then the production of a test tube produced with the new method is described. Quality control and geometric measuring are also described.

3.1 Filament Winding

Fiber strands are spooled on large bobbins and placed in a back tensioning system. The back tensioning system assures that the fiber has a constant tension during winding. Fiber tension assures that any excess epoxy is squeezed out when the strand is wound on the mandrel. High fiber tension generally leads to a higher fiber volume fraction as the plies are compressed more [36].

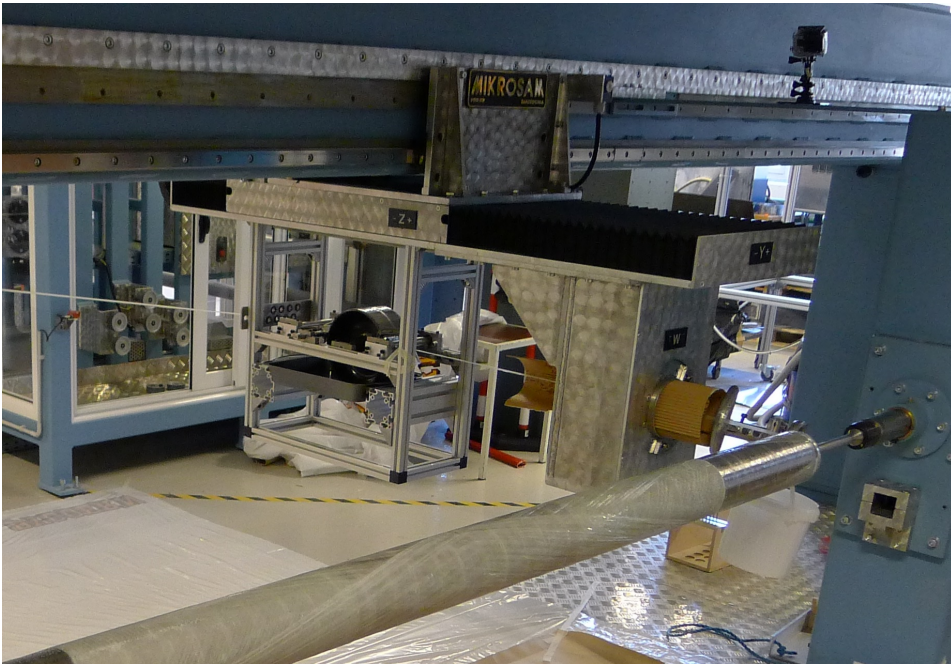
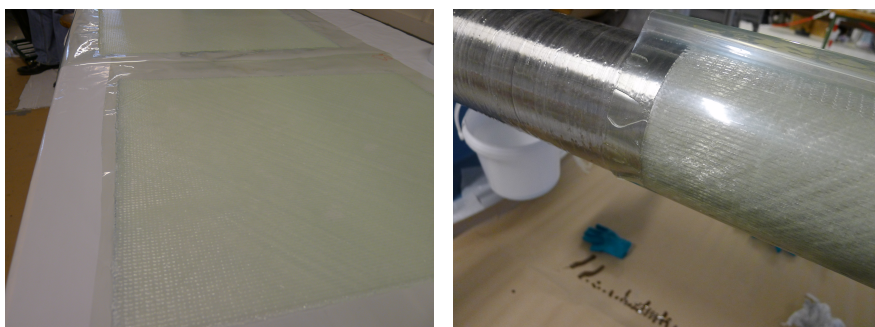


FIGURE 3.1: Filament winding, resin bath to the left, winding head and mandrel.

The fibers are then impregnated with epoxy in a resin bath. The amount of resin applied to the strands can be controlled by adjusting the epoxy film thickness on a wheel the strand passes over. The resin bath is to the left in Figure 3.1.

Wetted fibers then go to the winding head. The winding head, seen to the right in Figure 3.1, is controlled by a CNC system and moves in synchronization with the mandrel in a pre-programmed path that ensures the correct fiber angle.

Filament winding is suitable for serial production as it can be highly automated and produce products with consistent production tolerances. Fully automated winding machines capable of high volume production are available on the market today [35].



(A) Wetted mats

(B) Mat with plastic on mandrel.

FIGURE 3.2: Mat application

A limitation with filament winding is its inability to change winding angle over a short distance without any support structure to wind the fiber around. It is impossible instantly change winding angle without a transition [35]. The length of the transition depends on the slipperiness of the fiber strands, as friction is necessary. A slippery stand requires a transition zone that is quite large compared to the mandrel diameter. It is therefore impossible to add more fibers, with a different angle than approximately 90° , to only a section of the tube without a thicker transition outside the area. It is therefore unfeasible to reinforce only certain sections with the traditional filament winding method.

The new method diverges from the standard filament winding as it utilizes fiber mats to produce different layups along the length of the tube.

3.2 Tube and end fitting production

The production of a sample tube with the new method consists of several steps: winding, application of mats, cutting, bolt hole drilling, hub fitting and liner application. It is presented here in a stepwise chronological order.

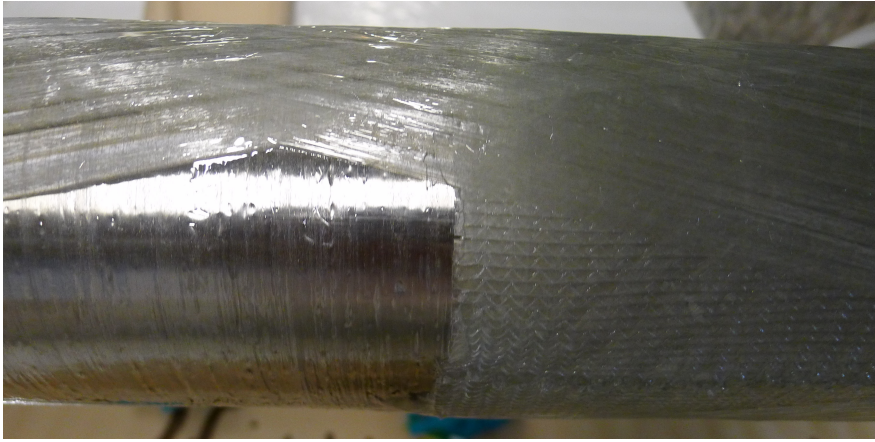


FIGURE 3.3: Helical winding over a mat.

A mandrel with 100 mm diameter, 2000 mm cylindrical length and spherical end caps was fitted in the winding machine. The mandrel was waxed with two layers of Zywax Flex-Z 3.0 [37] and one layer of SVAS release wax.

Epicote Resin MGS RIMR 135 and Epikure Curing Agent RIMH 137 were used in a mixing ratio of 100:30 [28]. The epoxy was used both for the mats and the winding.

Fiber paths were generated with the computer program Winding Editor made by Microsam. Bandwidth used in the program was 6 mm for the hoop plies and 5 mm with the helical plies.

The inner hoop layer and the 12.7° layer were wound with a fiber tension of 15 N. The three outermost hoop layers were wound with a fiber tension of 35 N to minimize the birding of the helical ply. This problem is described in Section 2.8. A summary of the production parameters are listed in Table 3.1

The mats were pre-cut to fit the length and estimated diameter, placed on plastic sheet and wetted with epoxy using a brush. Wetted mats are shown in Figure 3.2a. The mats were then wrapped around the mandrel with the plastic the outside on as shown in Figure 3.2b. The width of the mats

TABLE 3.1: Production summary. Letters under section refers to letters in Figure 2.3

Ply nr.	Fiber angles [deg]	Method	Joint placement	Fiber tension	Sections Fig. 2.3
1	[90]	wound	-	15 N	A,B,C,D,E
2-4	[-45/45/0]	mat	0	-	B,C,D,E
5	[±12, 7]	wound	-	15 N	A,B,C,D,E
6-8	[0/45/-45]	mat	180	-	C,D,E
9	[90]	wound	-	35 N	A,B,C,D,E
10-12	[0/45/-45]	mat	90	-	D,E
13	[90]	wound	-	35 N	A,B,C,D,E
14-16	[0/45/-45]	mat	270	-	E
17	[90]	wound	-	35 N	A,B,C,D,E

were cut according to the estimated diameter to produce axial butt joints between the mat edges.

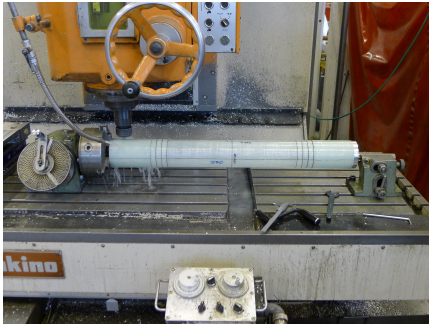
All the mats was placed with the axial joint between the mat edges approximately 90° apart, with the lengthwise placement and direction according to Figure 2.3 and Table 3.1. Before the next layer of winding as much excess epoxy as possible were squeezed out of the mats and the plastic sheet removed. It was not a problem to get the wound fiber strand to "climb" on to the newly applied mats. The mat edges was nicely covered by the wound strand without any special handling. Winding the helical ply over a mat is photographed in Figure 3.3. As the production went on it became clear that the laminate became thinner than expected as the outermost mat overlapped instead of producing a butt joint.

When the hoop plies were wound over the mats, a wake of excess epoxy formed in front of the strand. The mat was lifted from the ply underneath by the wake. This could have resulted in some misalignment of the mats. After each ply of hoop winding, any excess epoxy was scraped off.

The tube and mandrel were left rotating in the winding machine for 24 hours and then post cured in a oven at $60^\circ C$ for 15 hours as recommended in the Technical Data Sheet [28]. After curing, a pointy measurement pin



FIGURE 3.4: Finished tube before cutting.



(A) Drilling setup



(B) “Glass and tile” drill bit

FIGURE 3.5: Bolt hole drilling

was fitted to the winding head and used for measuring out markings for cutting and placement of strain gauges on the sample tube.

The ends of the wound tube were cut off and the mandrel removed in a mandrel extractor.

The finished tube before cutting can be seen in Figure 3.4

With the mandrel removed, the pipe was cut at the previously made marks in a band saw.

Bolt holes were then drilled in a CNC controlled mill with a partitioning head. No special caution was taken to avoid bolt holes on the mat joints. The drilling setup can be seen in Figure 3.5a. A “glass and tile” drill bit, seen in Figure 3.5b, was used with a federate of 10 mm/min together with a water based cooling liquid. The holes had no visual signs of delamination after drilling.



FIGURE 3.6: Bolt assembly. From the top: Hub, bushing, washers, screw head.

3.3 End fitting connection

The hubs were fitted one at a time. The inside of the tube was sanded with 220 grit sand paper and degreased with acetone. The hubs were degreased only. Axson UR 3435/3442 polyurethane was applied to the outer surface of the hub and the hub inserted in to the tube before bushings and bolts were fitted. M8 bolts, with internal hexagon head, of 12.9 quality, according to DIN-912 were used. 45mm long bolts with a 12 mm long straight shaft were cut down to 22 mm to fit the threaded holes in the hub. SKF composite bushings # CM 081010 E was inserted in to the bolt holes and two washers were used as spacers between the bolt head and the bushing. The assembly without the tube can be seen in Figure 3.6. The bolts were finger tightened to assure that the screw heads seated against the bushing to prevent it from slipping out of the bolt hole during testing.

After all the bolts and bushings were in place, the tube was suspended from the ceiling with the freshly fitted hub down. This placed the joint in slight tension while curing. This was done to seat the bolts and bushings towards the bolt hole in load direction.

One of the finished end fittings may be studied in Figure 3.7.

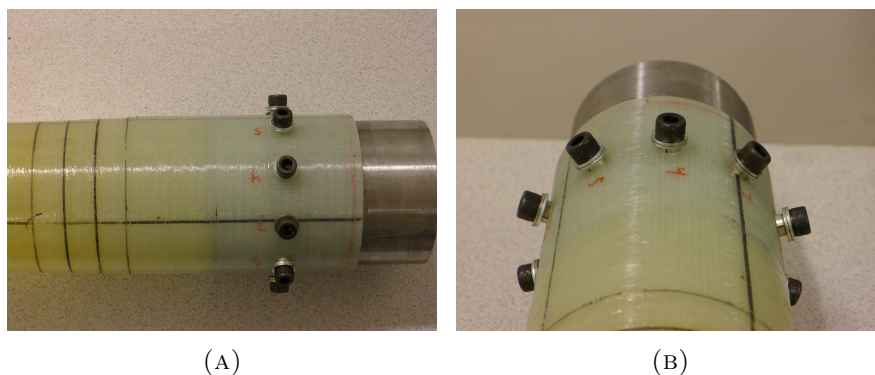


FIGURE 3.7: Finished tube and end fitting

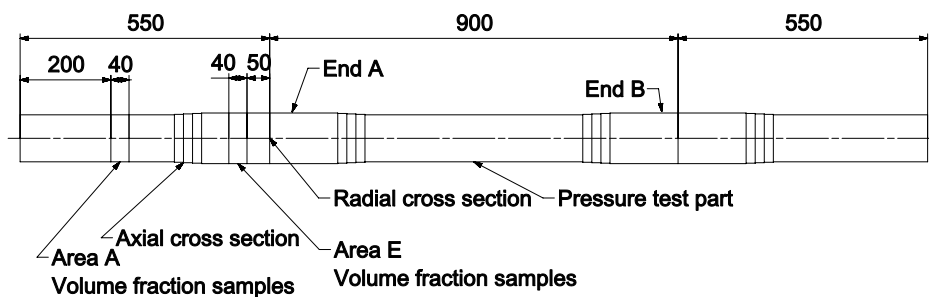


FIGURE 3.8: Cross section and specimen location on produced tube.

3.4 Liner

The "Safety and Quality Evaluation of Activities in the Laboratory and Workshop" form for the liner application can be found in Appendix D. 400 g of unhardened polyurethane, Axson 3435/3442 were mixed in a ratio of 100:80 according to the Technical Data Sheet [7], to make an approximately 1,6 mm thick liner. The uncured polyurethane was poured through an inlet hole in the hub and rotated in a lathe. The pipe was spun at 1400 RPM for 30 minutes to assure an even distribution of the liner while curing.

TABLE 3.2: Laminate thickness area A

Laminate thickness	
Average = t_A	1,74 mm
Max	1,79 mm
Min	1,65 mm
Standard deviation	0,050 mm

TABLE 3.3: Laminate thickness area E

Laminate thickness	
Average = t_E	3,99 mm
Max	4,11 mm
Min	3,86 mm
Standard deviation	0,087 mm

3.5 Geometric measuring of finished tube

The laminate thickness was measured at both ends of the pressure test piece and on one edge of the cut offs. The measurements were done with a digital caliper every 45° around the circumference. Results are listed in Table 3.2 and Table 3.3.

The filament wound ply thickness was found by dividing the thickness of area A (with pure filament wound material) with the number of plies. This results in an average ply thickness for wound plies of 0,29 mm.

The thickness of the wound plies was subtracted from the thickness of area E and divided by the number of mats giving an average mat thickness of 0,56 mm. To determine the thickness of each ply in the stitched mats, each plies area weight over the total area weight was used as a factor multiplied by the mat thickness. The area weights are listed in Table 2.3. This resulted in the $\pm 45^\circ$ plies being 0.14 mm thick and the 0° ply being 0.29 mm thick.

The produced layup are listed in Table A.2. Fiber fraction in the different angles for the produced layup listed in Table 3.4. Due to the fact that the mats became thinner than expected the ratio for the hoop fibers are rising.

TABLE 3.4: Fiber distribution of the produced laminate

Orientation	Fraction	Recomended fraction
0° and ±12,7°	42,8%	50%
±45°	28,9%	40%
90°	29,1%	10%

TABLE 3.5: Bolt hole diameter

Hole diameter	
Average	10,24 mm
Max	10,26 mm
Min	10,21 mm
Standard deviation	0,013 mm

TABLE 3.6: Edge distance

Edge distance	
Average	49,76 mm
Maxe	49,92 mm
Min	49,63 mm
Standard deviation	0,081 mm

To meet the recommendations one should have added more triaxial mats to the layup.

The bolt holes were measured with a bore gauge and the results are listed in Table 3.5. The bolt holes are larger than expected, resulting in a large clearance between the bushings and the laminate. With a 10 mm bushing the clearance is on average 0,24 mm or 240 μm . For aerospace application the typical clearance is 0 to +75 μm [38]. The clearance obtained here is then over three times as big. This is not a preferable, as it will lead to a more concentrated load on the laminate. The measurements indicate that the drill bit was not worn during the drilling of the 20 holes.

The edge distance was measured from the edge of the tube to the bolt hole edge with a digital caliper. Half of the bolt hole diameter previously measured was then added to obtain the edge distance to the center of the hole. The results are listed in Table 3.6. The edge distance is slightly

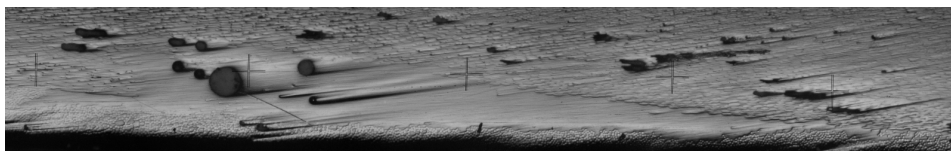


FIGURE 3.9: Microscopy of a helical ply wound over a mat edge. Inside of tube to the bottom of the photo.

smaller than targeted. This is probably due to a skew cut of the tube and not misalignment of the holes as the drilling process is more accurate than the cutting.

3.6 Microscopy of cross sections

Several cross sections were cut from the pipe to perform microscopy. The transition area with the mat edges and the axial butt joints on the mats are of interest as there are a larger chance of voids and areas without fibers there. The location of the cross sections are illustrated in Figure 3.8.

Figure 3.9 is a microscopy photo of the helical ply bridging from the mat edge on to the hoop ply below. As seen from the figure the $\pm 12,7^\circ$ ply form a nice smooth transition over the edge of the mat. The area between the ply is filled with epoxy, and but some circular voids are seen. This is a positive thing, as a triangular void with sharp corners would give a higher stress concentration than round bubbles.

In Figure 3.10 a microscopy photo of a radial cross-section. There are voids present in the whole laminate but more voids is found in the added mats. The using a brush to apply epoxy to the mats allow a lot of air to be trapped in the laminate and is the most likely cause of these voids. Filament wound material is known to generally have more voids than vacuum infused and prepreg materials. The material made here had no signs of anything unusual.

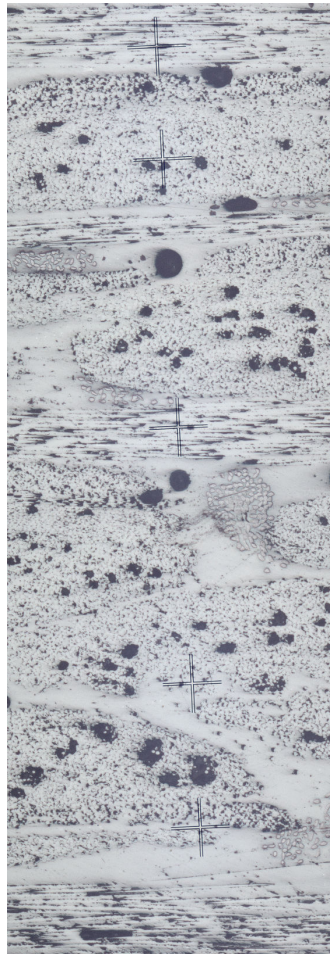


FIGURE 3.10: Microscopy of cross section. Inside of tube to the bottom of the photo.

3.7 Fiber volume fraction

As the fibers are the main strength and stiffness contributor in a composite material the fiber volume fraction, V_f , is an important parameter. To determine the fiber volume fraction, a burn off test was performed.

The pipe consists of two different materials and therefore have two different fiber volume fractions. The mats are compressed by the filament wound material on top and could therefore have a significantly different volume



(A) Sample nr. 6 before burn off (B) Sample nr. 6 after burn off.

FIGURE 3.11: Burnt off test sample

fraction than what is normal with a vacuum assisted resin infusion. It is therefore of interest to determine the fiber volume fraction both for the mats and for the filament wound material. To determine this six different samples were cut from the pipe. Three from area E with four added mats and three samples from area A with pure filament wound material. The samples were cut according to Figure 3.8 at 45, 135 and 225 degrees to avoid the mat joints.

The specimens were weighed and placed in small ceramic cups. The epoxy was burned off in a furnace at 500°C for 240 minutes. One cup and sample, before and after burning, is presented in Figure 3.11. After burn off, the samples were weighed again and the weight fraction, w_f , could be determined. As we knew the density of both epoxy and fibers from datasheets [6, 26, 28] the weight fraction was recalculated into volume fraction, V_f . The fiber volume fraction is assumed to be constant over the thickness. The tube was made with two different fiber tensions which could have led to different volume fractions [39].

The rule of mixture was used with the thickness measured on area A and E to determine the V_f for the added mats. In Equation 3.1 t_A is the thickness of

TABLE 3.7: Fiber volume fractions

	Wound	Wound and mat	Mat
Area	A	E	
$V_{f \text{ average}}$	61,6 %	58,8 %	56,6 %
SD	0,07	0,08	

the area A with pure wound material and t_E the thickness of section E with four mats and the same wound material as in section A. Using Equation 3.1 fiber volume fraction for the mats was obtained.

$$V_{f \text{ mats}} = \frac{V_{f \text{ E}} - \frac{t_A}{t_E} V_{f \text{ A}}}{1 - \frac{t_A}{t_E}} \quad (3.1)$$

The calculated average fiber volume fraction for the mats $V_{f \text{ mats}}$, after Equation 3.1 is then 56,6%, which is the same as a good quality vacuum infused laminate.

The measured V_f is further reduced by the void content as the burn of test assumes that no voids are present in the laminate.

The measured fiber volume fractions are on the high side for filament winding and very good for mats when compared to hand layup and vacuum assisted resin infusion.

3.7.1 Scaling of material properties

Strength and stiffness in fiber direction is linearly related to the fiber volume fraction. One can therefore scale the material properties obtained with one fiber fraction to a laminate with the same materials, but a different fiber volume fraction. Material properties in fiber direction, listed in Table 2.2 and 2.4, were scaled to the obtained fiber volume fractions after Equation 3.2. The results are listed in Table 2.2 and 2.4.

TABLE 3.8: Expected failure pressures and axial loads of the produced laminate.

	Cosine bearing load and $K_T = 4$		Constant bearing load and $K_T = 3$		Location
	Pressure [Mpa]	Axial load [kN]	Pressure [Mpa]	Axial load [kN]	
Y_T	2	17	3	23	Net-section
Y_C	7	60	12	94	Bearing
S_{XY}	10	81	14	107	Net section
X_C	11	83	16	130	Bearing
X_T	17	132	22	174	Net-Section

$$\text{New value} = \frac{V_{f \text{ new}}}{V_{f \text{ old}}} \text{Old value} \quad (3.2)$$

In Equation 3.2 New value is the material property wanted with a new volume fraction $V_{f \text{ new}}$. $V_{f \text{ old}}$ is the volume fraction from the material where the property "Old value" was obtained.

3.8 Laminate theory

The same approach as described in Section 2.10 was used to determine the ply failure pressures for the produced laminate. The produced laminate thickness and scaled material properties was used.

Being equally conservative (or no conservative) as in Section 2.10 gives the produced laminate a design failure pressure of 13.3 MPa corresponding to an axial load of 108.3 kN.

Chapter 4

FEA model

A simple Finite Element Analysis, FEA, model was made to compare experimentally measured strains in the tube with a model. Strains were analyzed close to the bolts, but it was difficult to use a FEA model to determine the strength of the bolted joint, because a FEA model without a material damage model creates high stress concentrations near the bolt hole that do not converge. It was beyond the scope of this thesis to model local damage development and estimate the strength of a bolted joint from a FEA model.

A simple shell model for the produced tube has been made as a comparison for the experimental data that are obtained some distance from the bolt hole.

4.1 Geometry, elements, mesh and solver

Thickness measured on the produced tube was used to find the midplane diameters and a 3D shell model was established. Only 1/20 of the tube was modeled, 1/10 of the circumference (36°) and 1/2 of the length. Cyclic symmetry was exploited. The shell was set to represent the midplane of the laminate and the transition between the different thicknesses was modeled

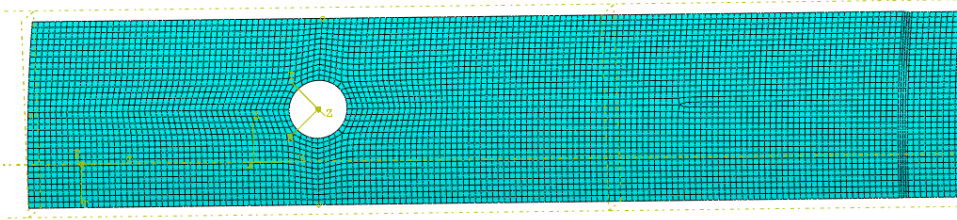


FIGURE 4.1: Mesh around bolt hole.

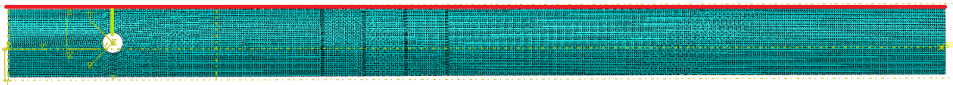


FIGURE 4.2: FEA model; Axial edge along red line and net section along green line.

with 10° fillets in the shell. A detailed drawing of the shell can be found in Appendix C.

Abaqus FEA software was used for the simulation. 1 mm, S8R elements, with structured meshing were used. S8R elements are eight noded quadratic shell elements with reduced integration and hourglass control [40]. Engineering judgment was used when selecting the element size and it is seen as sufficiently small to determine strains at some distance from the bolt hole. A full FE analysis would require a mesh sensitivity study. The purpose of this analysis was to get a estimate of the strain some distance from the bolt hole, as a comparison for experimental results. The mesh sensitivity was therefore not studied further. The mesh around the bolt hole can be seen in Figure 4.1 and the whole model in Figure 4.2.

4.2 Layup and material properties

Material properties listed as scaled in Table 2.2 and 2.4 were used. The layup is specified in Table A.2 and the areas for the different layups is

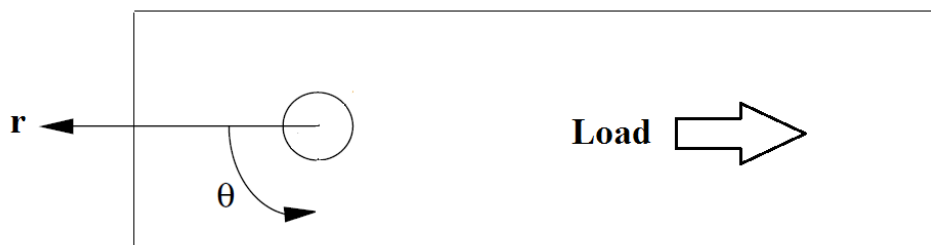


FIGURE 4.3: Bolt hole coordinate system. Figure adapted from Aktas and Husnu Dirikolu [4]

illustrated in Appendix C.

4.3 Loads, boundary conditions and solving method

Boundary conditions for rotational symmetry were applied at the axial edges and plane symmetry conditions, except axial deformation, at the edge towards the center of the tube.

The bolt hole was simulated with the help of a local cylindrical coordinate system with the Z axis going through the center of the hole, as illustrated in Figure 4.3. The hole edge from $\Theta = +90^\circ$ to $\Theta = -90^\circ$ was radially constrained to simulate the bushing. Bushing stiffness was not taken into account in this simple model. This boundary condition simulates a bolt with slip conditions around the circumference. The laminate is allowed to slide around the bolt in Θ direction with no friction. This method of simulating the bolt has been used by Aktaş et al. [41] before with good results combined with the design method described by Camanho and Lambert [17].

The nodes at the edge towards the center of the tube were linked to a common reference point. The load was then applied as a displacement in axial direction. The displacement was set to 5 mm simulating a 10 mm crosshead displacement (the model is half the length of the sample tube).

The Abaqus linear solver was used [40]. Any geometric nonlinearities were not taken in to account as small deformations is assumed.

4.4 Output

The results from the FEA analysis are used as a comparison against the experimental results. Axial and hoop strains were extracted along the axial edge of the model indicated by a red line in Figure 4.2 and axial strains in the net section, indicated by a green line. The results were taken from the very outside of the laminate as the experimental measurements are taken on the outside of the tube.

4.5 Force and displacement scaling

It is possible to directly scale the results such as strain for various displacements or loads as desired since the model is solved linearly.

Scaling of strain is done using equation 4.1 or 4.2 .

$$\epsilon_{Wanted} = \frac{F_{Wanted}}{F_{FEA}} \epsilon_{FEA} \quad (4.1)$$

$$\epsilon_{Wanted} = \frac{\delta_{Wanted}}{\delta_{FEA}} \epsilon_{FEA} \quad (4.2)$$

Subscripts "Wanted" is the load or displacement the result is wanted for while subscripts "FEA "is the magnitude of the result in the FEA result file that is scaled.

When comparing the FEA result to experimental data either force or displacement scaling can be beneficial.

Chapter 5

Experimental testing

Both a pressure test and a tensile test of the tube with end fittings was conducted.

5.1 Instrumentation

The tube was instrumented using two different technologies for strain measurements; traditional strain gauges and a Optical Backscatter Reflectometer, OBR. The OBR uses an optical fiber glued to the sample to measure the strain. The strain is measured by shooting laser light into the fiber and measure different things on the light that is reflected back from inside the fiber [42]. A limitation to the method is the large amount of data created for each measurement. Data transfer limitations between the OBR and the computer hard drive makes a high sampling rate impossible. The sampling rate for the OBR is therefore very low compared to what is possible with strain gauges. Another limitation is OBR's lack of ability to measure strain on moving samples. The best results are obtained while measuring in a static state or a very low strain rate.

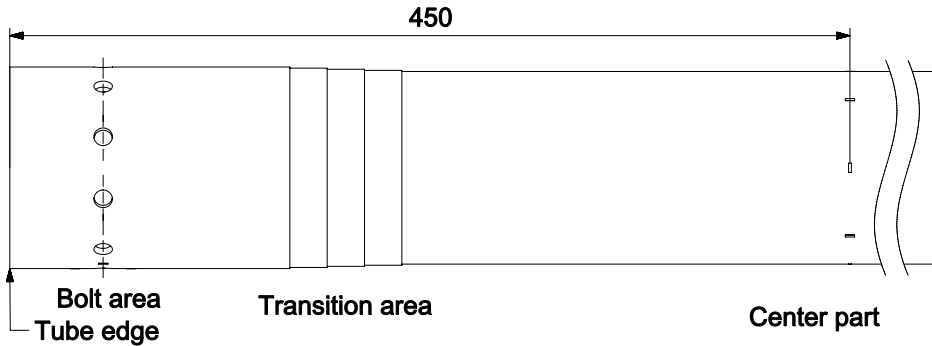


FIGURE 5.1: Instrumentation areas.

Results from the OBR can be interpreted as a continuous row of strain gauges overlapping each other. In the software following the OBR, one can set the gauge length and spacing of the gauges. A gauge length of 5 mm and a spacing of 0,6 mm were used. Unfortunately measurement noise can be a problem at high strains as the fiber can release from the surface. The Optical Backscatter reflectometer is not further described here. More information is available in the master thesis by Håheim [42].

Strain gauges from TML denoted FLA-5-11-1L were used. It is a general purpose 120 Ω strain gauge with a gauge size of 5x1,5 mm [43].

5.1.1 Center part

To detect any bending in the sample and measure the deformation in the center part of the tube, eight strain gauges were placed in the center of the tube. Two strain gauges in hoop direction at 0° and 90° degrees denoted

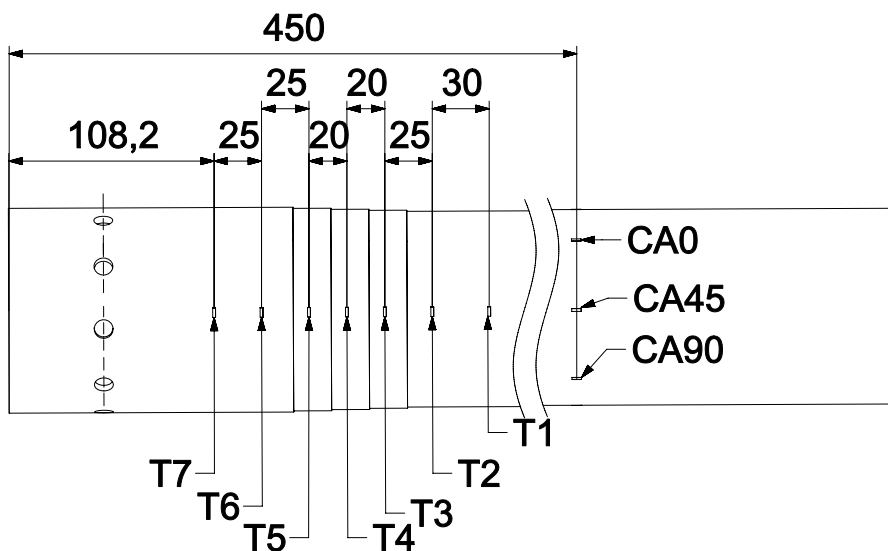


FIGURE 5.2: Strain gauges T1-T7, C0, CA45 and CA90. Strain gauges illustrated as squares.

CH0 and CH90 and six in axial direction at 45° , 135° , 180° , 225° , 270° and 315° denoted CA45 to CA315 according to their placement.

5.1.2 Bolt area

The load distribution between the bolts is of interest as the strain in the net section between the bolts is related to how the bolts are loaded and how evenly the load is distributed. This is interesting to know as it can be a function of both design and fabrication tolerances. The strain measurements between the bolts was done with the OBR. The optical fiber was glued in zigzag between the bolts and glued down along the center of each net section as illustrated by black lines in Figure 5.3.

As a reference to the OBR measures four strain gauges were placed around one bolt hole as illustrated in Figure 5.4.

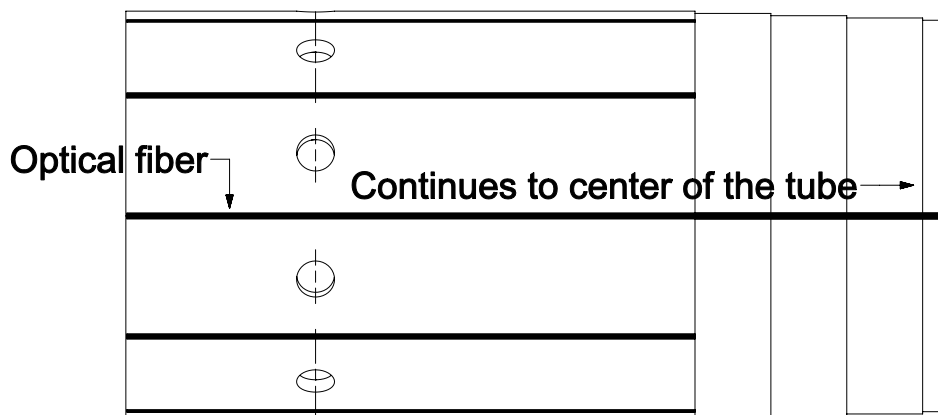


FIGURE 5.3: Placement of optical fiber between bolt holes. The fiber was glued to the tube along the black lines.

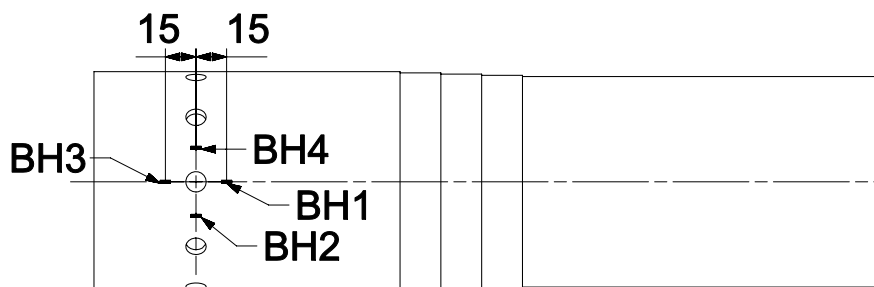


FIGURE 5.4: Strain gauges BH1-BH4 around a bolt hole.

5.1.3 Transition area

To measure the deformation in the transition, strain gauges were placed in hoop direction as illustrated in Figure 5.2. These gauges are denoted T1 to T7 going from the center of the tube towards the end. In addition the optical fiber was glued all the way to the center of the tube two different places to measure the axial strain as illustrated in Figure 5.3.

5.2 Pressure test

The "Safety and Quality Evaluation of Activities in the Laboratory and Workshop" form for the pressure test can be found in Appendix D. A high pressure water pump was connected to one end of the tube and a digital pressure gauge was connected to the other end. The tube was filled with water and the air vented out. The pipe was then placed in a thick steel tube, closed with a lid in one end and the other end placed against a wall to prevent any flying debris in the laboratory. The setup before it was placed in the steel tube can be seen in Figure 5.5.

The pressure was raised slowly while strain and pressure data was logged. Due to limitations in the equipment only gauges CH0, CH90, CA 180, CA 270 and T1-T7 were logged together with the OBR during the pressure test.

5.3 Tensile test

Due to a lack of good results from the pressure test, a tensile test of the tube was conducted. The "Safety and Quality Evaluation of Activities in the Laboratory and Workshop" form for the tensile test can be found in Appendix D. A tensile test will replicate the axial force on the hub normally imposed by the internal pressure as illustrated in Section 1.2 and the end fittings axial strength can be tested.



FIGURE 5.5: Pressure test setup.

5.3.1 Test setup

To connect the end hubs to a test machine two steel bars were centered on the inlet hole in the hubs and welded on. This was done while the composite tube was connected. Wetted rags were used to cool down the hub and composite tube while welding. The hub near the tube was never too hot to touch bare handed so the tube never experienced any heat that should affect the material properties. The modified end fitting can be seen in Figure 5.6.

The logging equipment limited the number of strain gauges it was possible to log. Only gauges T2-T6, CA45-CA315, BH2 and BH4 were logged during the test.

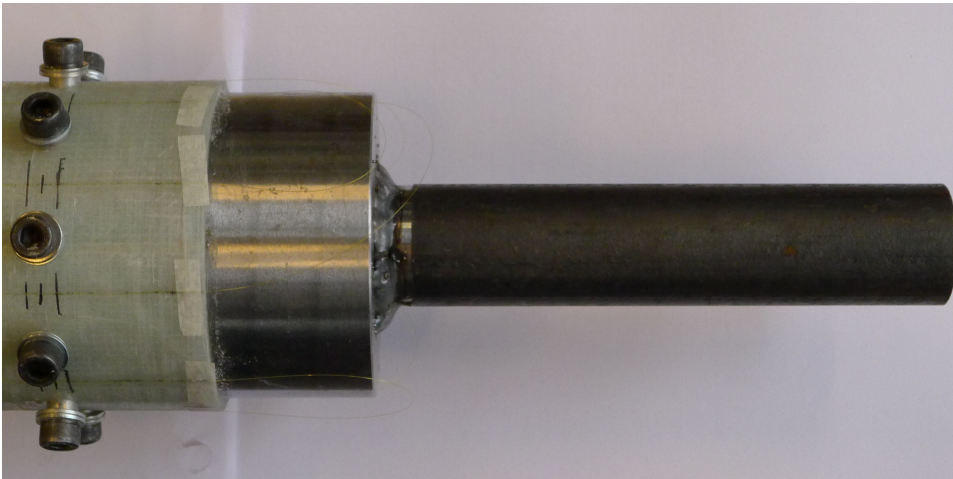


FIGURE 5.6: Modified end fitting for tensile test, with optical fiber glued on.

5.3.2 Strain rate

The test was conducted in a 1000 kN Schenk test machine seen in Figure 5.7, with a constant crosshead speed of 0,01 mm/s. As a reference, “ASTM D5961/D5961M-10: Standard test method for bearing response of polymer matrix composite laminates”, procedure A, uses a standard test specimen that is 117 mm from the edge to the hole and suggests to use a crosshead speed of 0,033 mm/s [21]. The optical backscatter reflectometer requires a low crosshead speed to measure correctly, so a lower speed was used.

The crosshead was stopped at 11,3 mm displacement, kept at 11,3 mm for 2,4 minutes, and then lowered at a speed of 0,01 mm/s until the sample was unloaded.

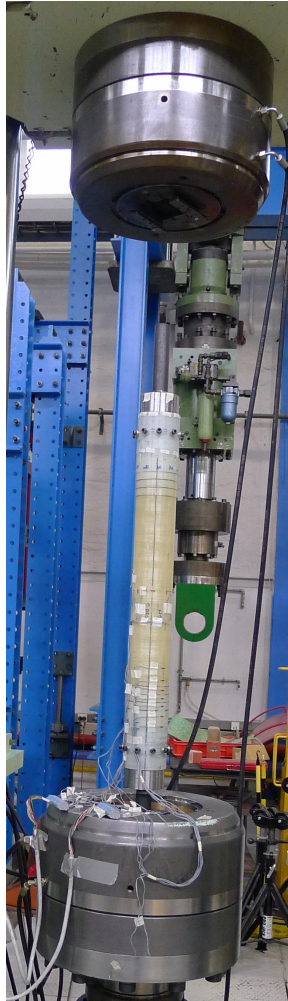


FIGURE 5.7: Tensile test setup.

Chapter 6

Results

Results from the FEA model, pressure test and tensile test are treated in this chapter.

6.1 FEA modeling

Figure 6.1 shows the axial strain along the edge of the model, illustrated by a red line in Figure 4.2. The curve shows large discontinuities in the

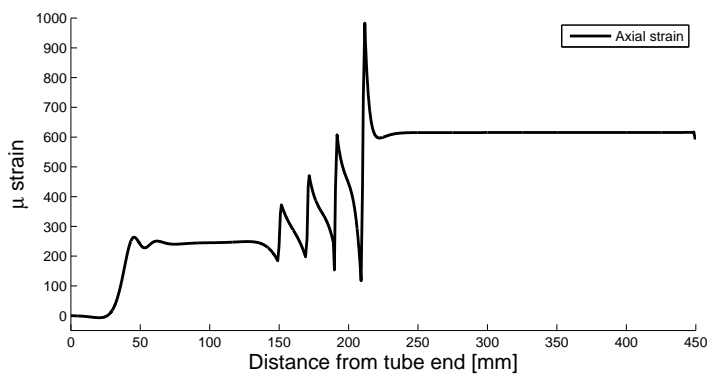


FIGURE 6.1: Strain in axial direction at a crosshead displacement of 0,8 mm.

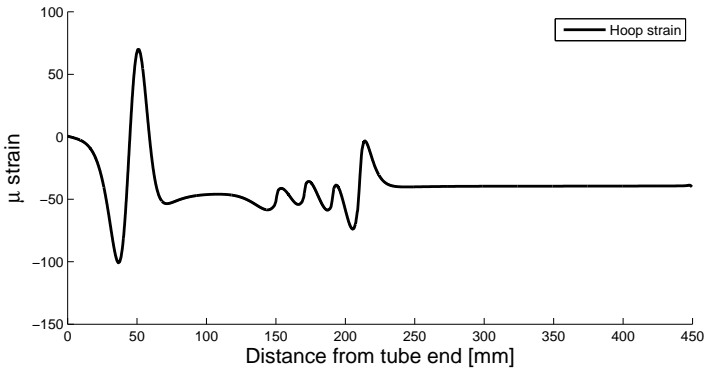


FIGURE 6.2: Strain in hoop direction at a crosshead displacement of 0,8 mm.

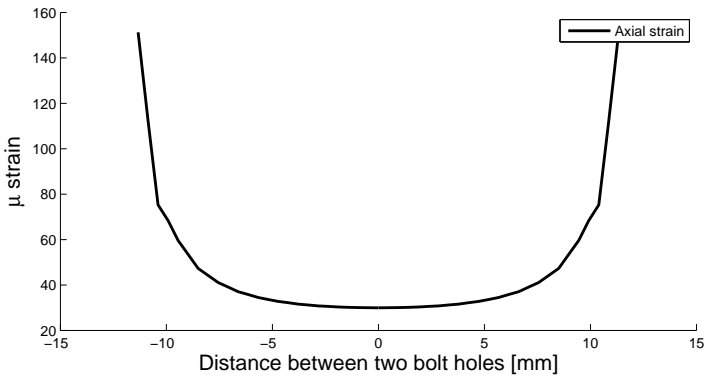


FIGURE 6.3: Axial strain in one net section between two bolts at a crosshead displacement of 0,8 mm.

transition zone where the layup is changing.

Hoop strain along the axial edge of the model, illustrated by a red line in Figure 4.2, is plotted in Figure 6.2. Figure 6.2 shows large rapid changes in strain close to the bolt hole and in the transition zone.

In Figure 6.3 the strain in the axial direction in the net section is plotted vs. distance from the midpoint between two bolt holes. The location is illustrated by a green line in Figure 4.2. As seen in the plot the strain is rapidly increasing towards the bolts while it is a relatively constant in the middle.

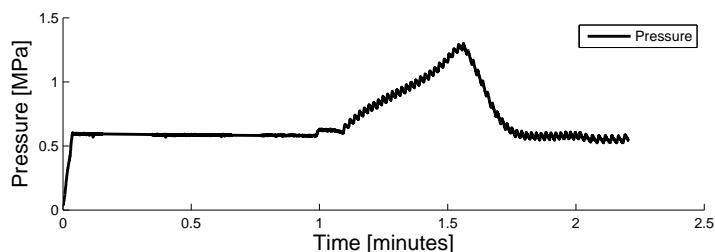


FIGURE 6.4: Pressure vs. time.

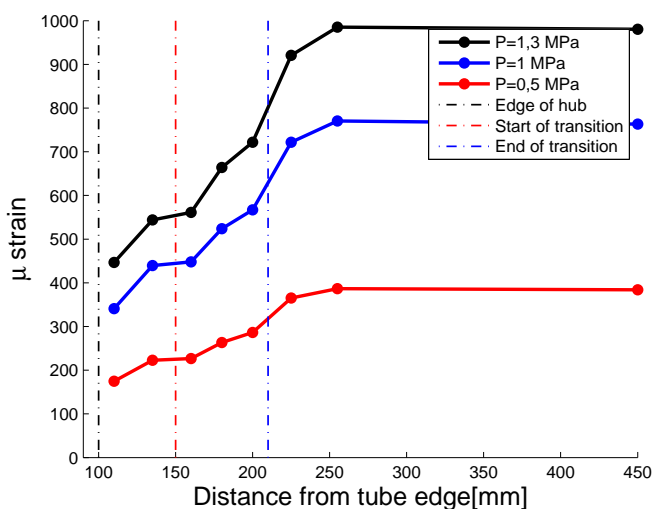


FIGURE 6.5: Stresses in hoop direction at transition area.

6.2 Pressure test

The pressure vs. time curve can be seen in Figure 6.4.

A maximum pressure of 1,3 MPa was measured.

After increasing the pressure to 1,3 MPa the tube was leaking as water was seen coming out of the test setup. The tube was removed from the test setup and visually inspected. The water was leaking out of two bolt holes.

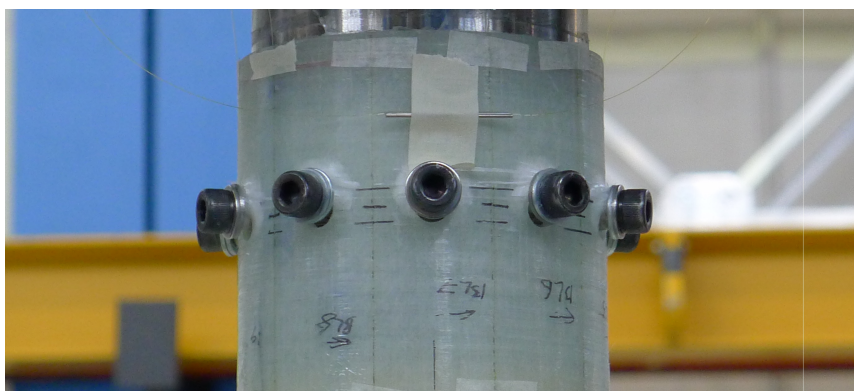


FIGURE 6.6: Bolts under load at a crosshead displacement of 11,3 mm.

In Figure 6.5 the strain in hoop direction for T1-T7 and the mean value of CH0 and CH90 are plotted against distance from the tube edge at different pressures. The measurements indicate linear response to increasing pressure.

6.3 Tensile test

There were uniform deformation and damage propagation around the bolts during the test. Both ends of the tube failed in bearing failure at all bolts. There were no visual difference between two ends. In Figure 6.6 some of the bolts are shown at the maximum displacement, 11,3 mm.

In Figure 6.7 one bolt is seen after unloading. The laminate is clearly pushed outwards on the bolt. The outermost hoop ply has fiber failure in the area just in front of the bolt. Delamination is seen in a half circle around the bolt hole in Figure 6.6 and Figure 6.7.

The tensile force and crosshead displacement is plotted against time in Figure 6.8. The maximum force was 96,16 kN and it was reached at a crosshead displacement of 8,02 mm after 13,4 minutes.

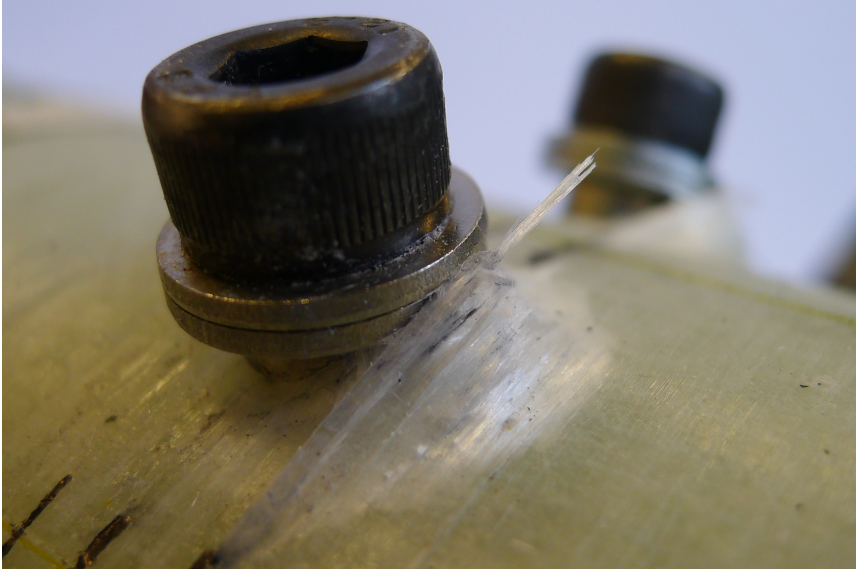


FIGURE 6.7: Bolt and tube after unloading.

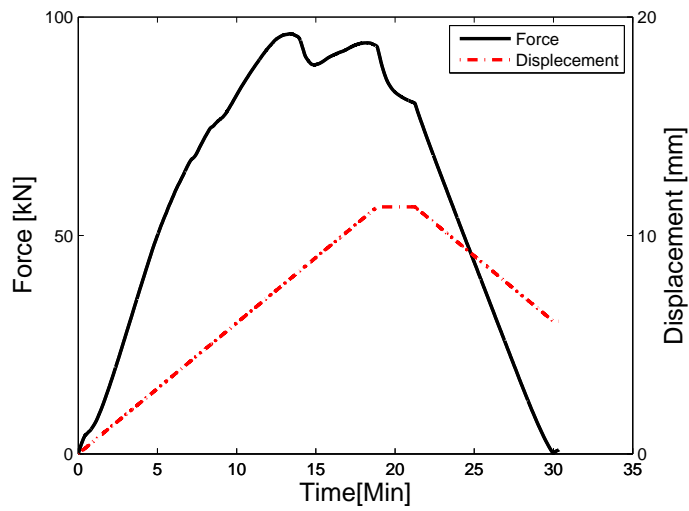


FIGURE 6.8: Force and crosshead displacement vs. time

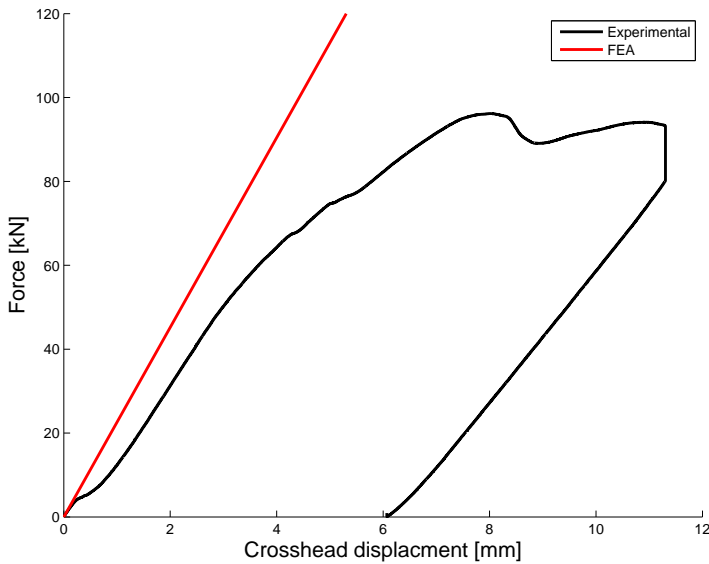


FIGURE 6.9: Force vs. crosshead displacement.

At a displacement of 11,3 mm the crosshead was kept stationary for 2,4 minutes and then unloaded. The force vs. time curve in the time where the crosshead displacement was kept constant shows a classical exponential relaxation response.

Force vs. displacement is plotted in Figure 6.9. It shows a linear deformation until a crosshead displacement of about 0,5 mm. Then a nonlinear more compliant part is seen until a crosshead displacement of about 1 mm. Then follows a linear part until a crosshead displacement of 4,25 mm. It is followed by two small nonlinear parts one starting at 4,25 mm and another at around 5 mm crosshead displacement. A larger nonlinear part follows towards the maximum load.

After the maximum is reached the force is reduced to 85 kN before it starts increasing again and reaches a second maximum of 94,1 kN. The unloading response is linear down to a displacement of about 6,3 mm where the sample was completely unloaded. The sample has become 6,3 mm longer during testing.

Force vs. displacement for the FEA model is plotted together with the experimental results in Figure 6.9. The FEA model has similar slope as the linear part of the experimental data.

6.4 Strain measurements

The location of the different strain gauges and the optical fiber is found in Section 5.1.

The outer ply of the tube is a hoop wound ply, with the fibers transverse to the load direction. Matrix cracking in the outer ply starts early in the test since the fibers are oriented transverse to the load direction. Matrix cracking damages the gauges glued on to the surface. This can be seen as rapid changes in strain. Measurements after such a rapid change are discarded.

Strain data from the FEA model are taken along the edge marked with a red line in Figure 4.2 at a location according to the placement of the strain gauges as specified in Section 5.1. Force and displacement scaling of the FEA results are done as described in Section 4.5. When force scaled FEA results are used the FEA data is plotted with the same force as the corresponding experimental data. The displacement of the FEA model is therefore different from the displacement of the experimental data despite being in the same plot.

6.5 Center part

In Figure 6.10 the strain in the axial gauges in the center of the tube are plotted against displacement. From about 1 mm crosshead displacement, the gauges show a linear response. The force scaled FEA result shows a stiffer behavior than the experimental results, seen as lower strains.

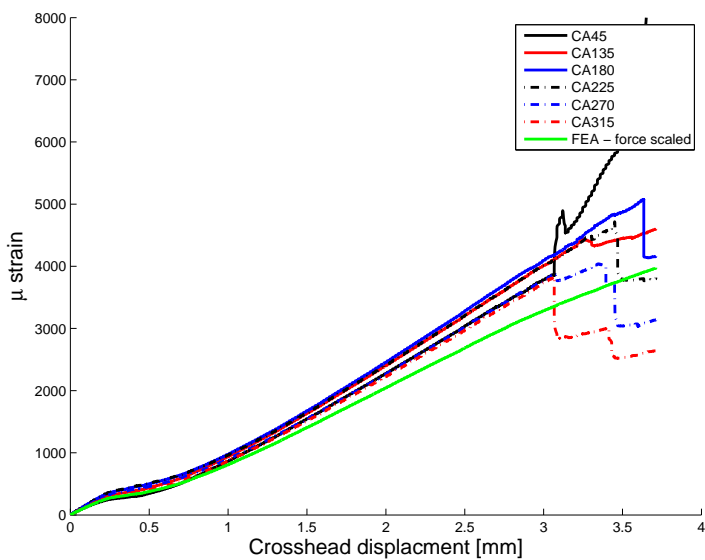


FIGURE 6.10: Axial strain at the center vs. displacement.

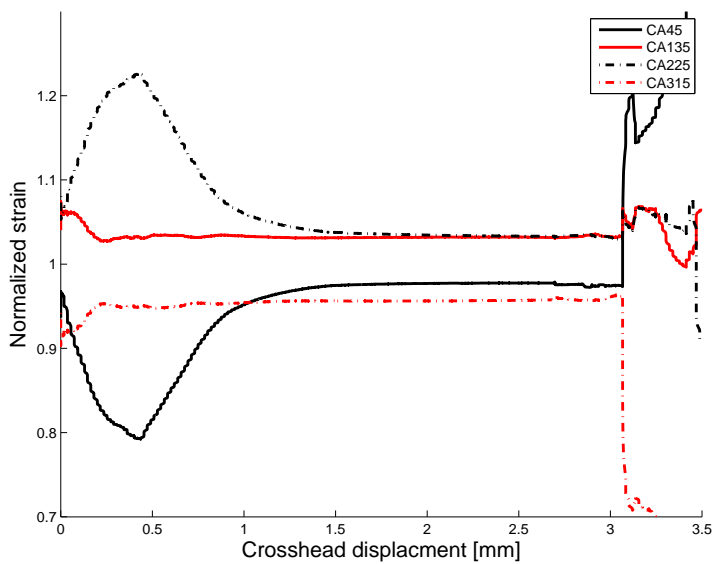


FIGURE 6.11: Strain for CA 45, 135, 224 and 315 normalized by the average strain vs. displacement.

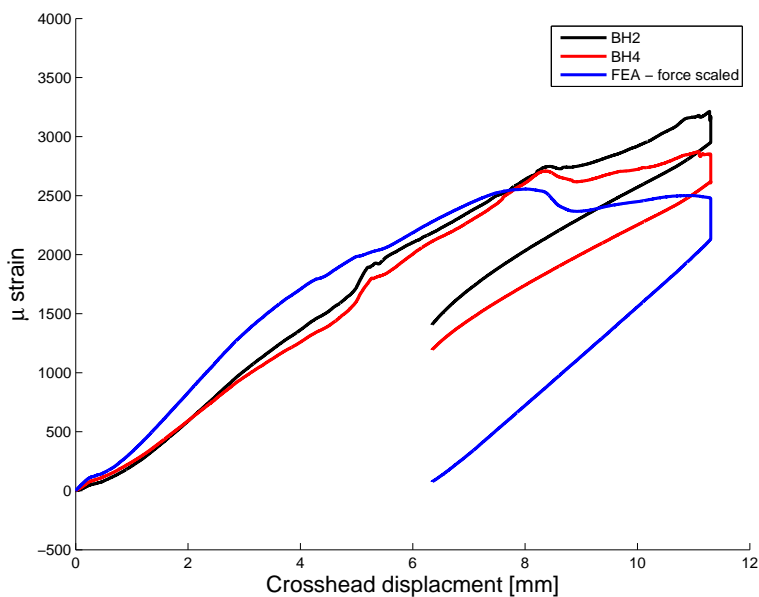


FIGURE 6.12: Strain at BH2 and BH4 plotted against displacement together with force scaled FEA results.

In Figure 6.11 the strain in four of the axial gauges at the center are normalized by the average strain. The results indicate that there are up to 20% difference in strain around the circumference in the beginning and decreasing fast to a constant difference of about 5-7%.

6.6 Bolt area

In Figure 6.12 the strain in the two strain gauges on each side of a bolt, BH2 and BH4 are plotted against crosshead displacement. Their response is almost the same during the whole tensile test. At 5 mm crosshead displacement, they both show a sudden increase in strain. The FEA model has a softer response than the experimental data.

In Figure 6.13 to 6.16 the strain measured by the OBR in the optical fiber between the bolts is plotted at four different crosshead displacements, together with the results from strain gauges BL2 and BL4. As seen from the

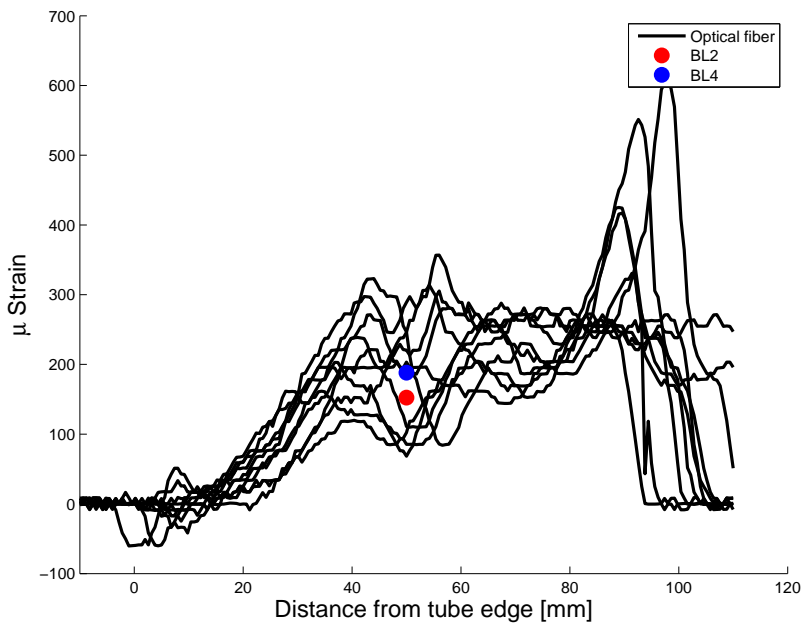


FIGURE 6.13: Strain in axial direction vs. distance from tube edge at a displacement of 0,8 mm.

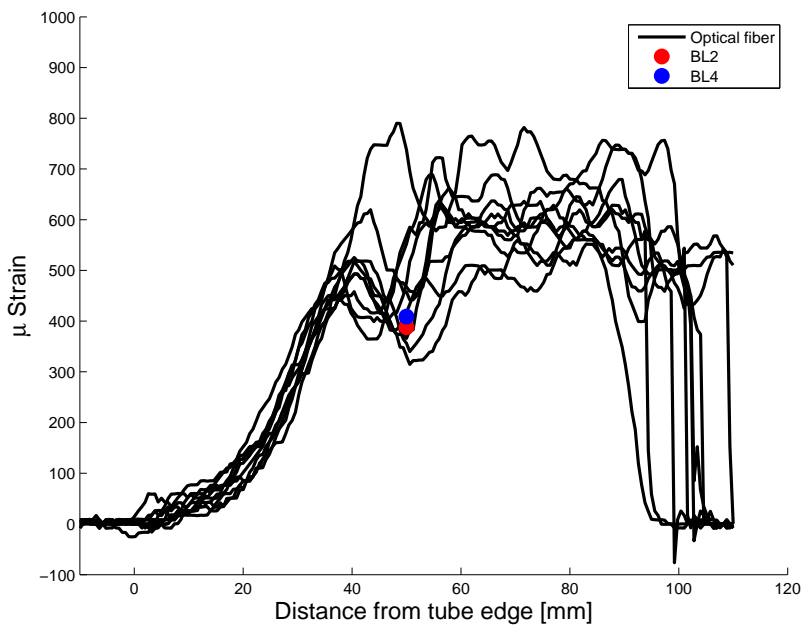


FIGURE 6.14: Strain in axial direction vs. distance from tube edge at a displacement of 1,5 mm.

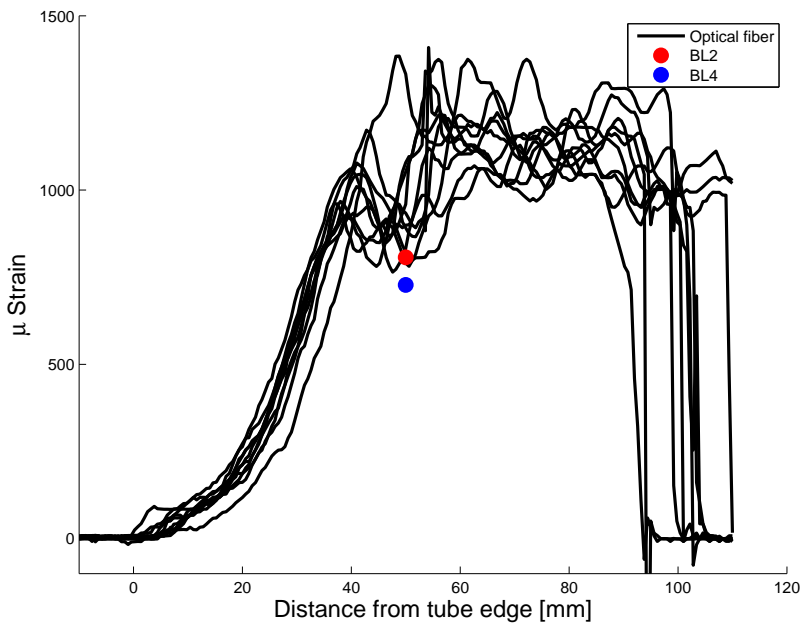


FIGURE 6.15: Strain in axial direction vs. distance from tube edge at a displacement of 2,5 mm.

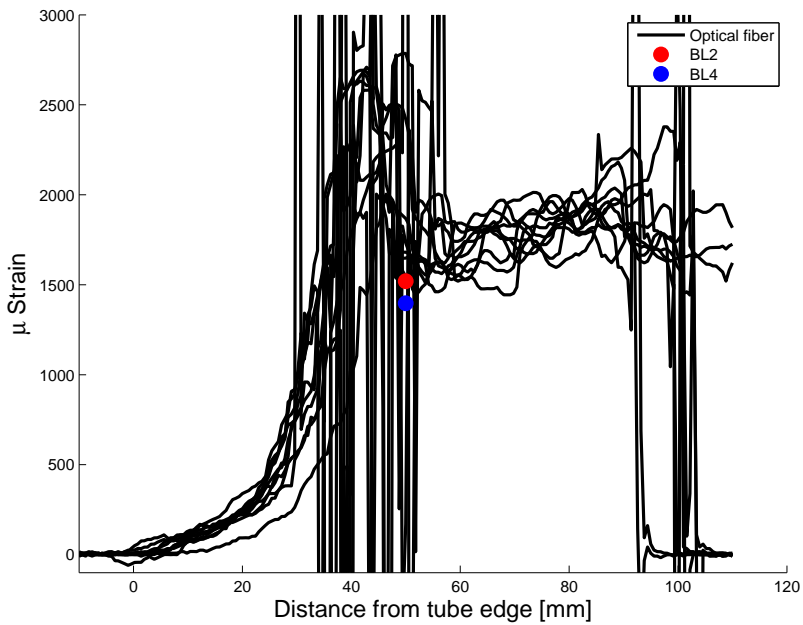


FIGURE 6.16: Strain in axial direction vs. distance from tube edge at a displacement of 4,5 mm.

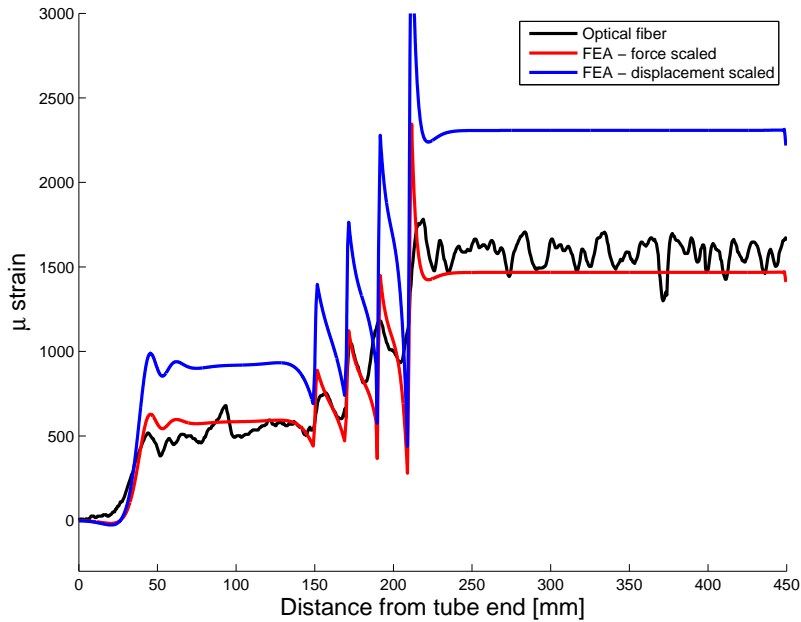


FIGURE 6.17: Axial strain in optical fiber and in FEA model at a crosshead displacement of 1,5 mm.

graphs the results have a lot of scatter making it hard to determine any difference between the bolts.

6.7 Axial strain, from tube edge to tube center

In Figure 6.17 and Figure 6.18 the axial strain, is plotted against distance from the tube edge, for various crosshead displacements. The strain measurements are taken from the optical fiber going all the way to the center of the tube. The results are plotted with displacement scaled FEA results and with force scaled FEA results.

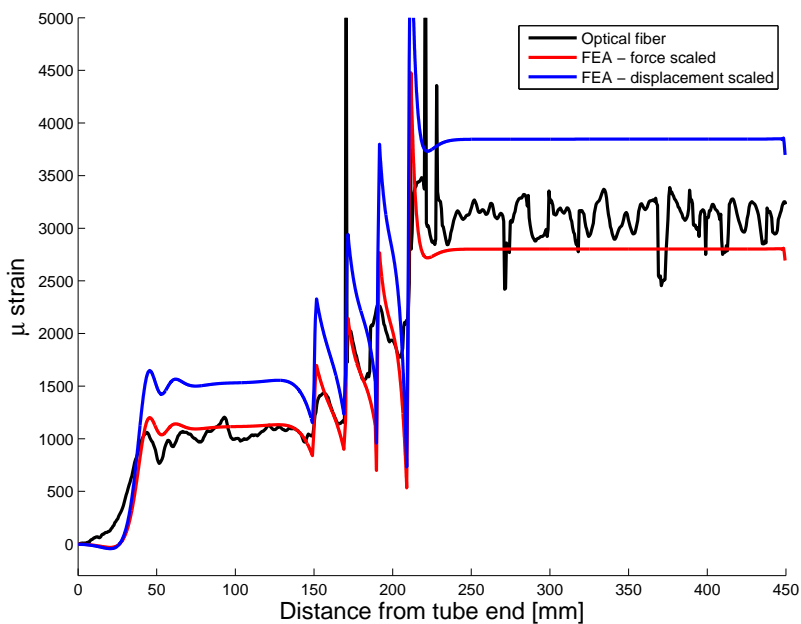


FIGURE 6.18: Axial strain in optical fiber and in FEA model at a crosshead displacement of 2,5 mm.

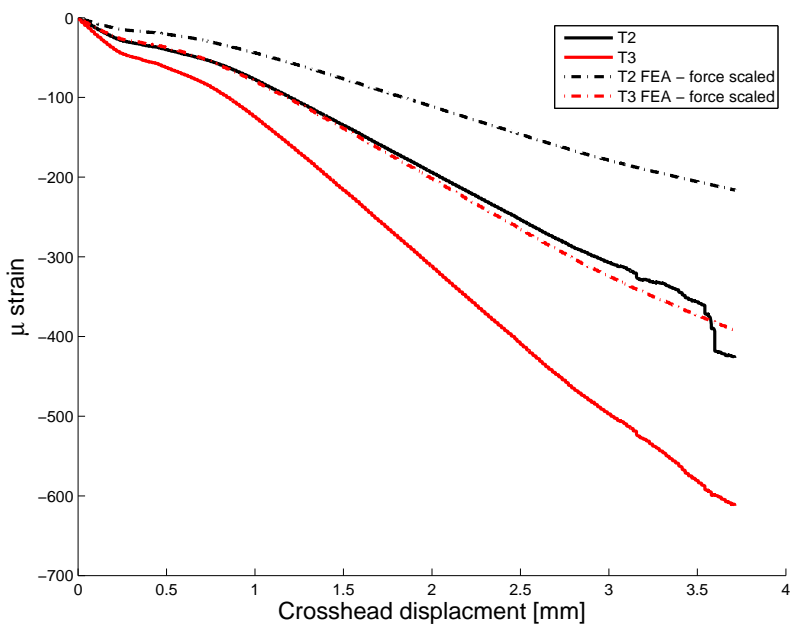


FIGURE 6.19: T2 and T3 vs. displacement, plotted with FEA results.

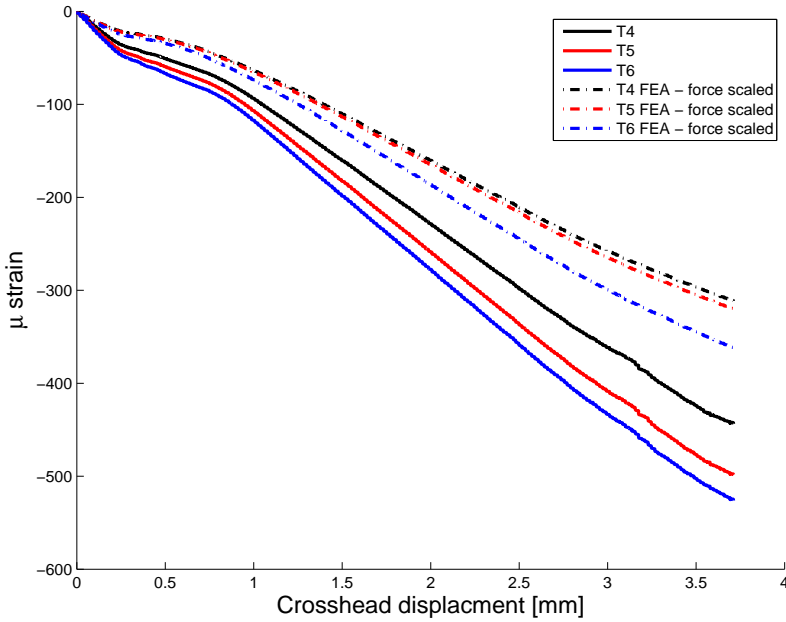


FIGURE 6.20: T4, T5 and T6 vs. displacement, plotted with FEA results.

6.8 Transition area

In Figure 6.19 and 6.20 the strain in hoop direction at the transition is plotted against displacement together with force scaled results from the FEA model. The force scaled FEA results shows a stiffer behavior than the experimental results.

6.9 Comparison between FEA and Experimental results

In Figure 6.21 the percent wise difference between the FEA results and experimental results are plotted using Equation 6.1

$$\%Difference = 100 \frac{\epsilon_{FEA} - \epsilon_{experimental}}{\epsilon_{experimental}} \quad (6.1)$$

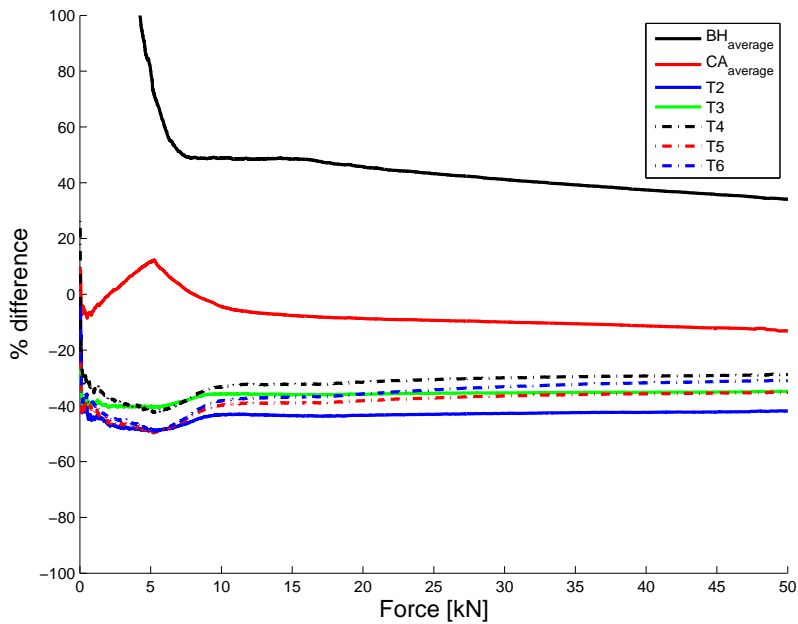


FIGURE 6.21: Percent wise difference between FEA and experimental results.

The FEA model predicts about 50% more strain compared to the BH gauges, 10% less strain in the center of the tube and 40% to little strain in hoop direction at in the transition.

Chapter 7

Discussion

Many aspects of the tube and end fitting have been explored.

7.1 Production

The production method was simple to use and produced an excellent composite tube.

The laminate became a thinner than expected, since the mats became only 0,562 mm thick. Due to this, the pre-cut mats were too wide resulting in an overlap instead of a butt joint of the outermost mat. Microscopy of the cross section indicated no big voids or fibreless areas near the overlap. As the true production thickness of the mats has been established this can be avoided in the future. The bolt holes had no signs of delamination after drilling. The holes had a larger than expected due to poor dimensional tolerance on the drill bit. As seen in Figure 6.9 the tube experienced initial yielding in the beginning of the tensile test. This shows that the bolts did not set against the bolt holes when the hubs were glued in, despite the axial tension applied by suspending the tube from the ceiling. The polyurethane liner was simple to apply and could be developed further to include a working sealing system.

7.2 Pressure test

The tube and end fitting obtained a maximum pressure of 1,3 MPa, resulting in a an average axial load of 0,1kN per bolt. The axial load is so small that the end fittings could have been supported by the polyurethane between the hub and tube instead of loading the bolts. Any measurements on the load distribution between the bolts is therefore considered invalid.

As expected edge effects are present although they disappear fast towards the center, as seen in Figure 6.5. The strain is close to the strain at the center only a few millimeters away from the transition. Towards the hub, the strain is rapidly decreasing.

7.2.1 Leakage

The end fittings were not disassembled to investigate the leakage. Further design and testing of a good sealing and liner solution were not in the scope of this work so the leakage was not inspected further.

The most likely cause of leakage is the expansion of the composite tube ripping the polyurethane in the tube-hub interface apart. As seen in Figure 6.5 the hoop strain only 10 mm away from the hub edge is 450 μ strain. The strain corresponds to a diameter increase of 0,045 mm (assuming a thin walled tube). For a thin adhesive layer between the hub and the tube even this small increase could have led to large strains in the polyurethane creating a crack the water could leak through.

7.3 Tensile test

Visula inspection of the tube during the test indicate that there are no large differences between the two ends. Large differences would be seen as non-uniform damage propagation or damage to only one end.

In Figure 6.8 a classical exponential relaxation curve is seen during the 2,4 minutes the crosshead displacement was kept constant. The stresses and strains around the bolt holes are inevitably very high as the laminate has experienced a bearing failure. It is likely that most of the relaxation happened near the bolt holes as this was the most stressed part of the tube.

The initial compliant part seen in Figure 6.9 is interpreted as the release of the polyurethane between the tube and hub. The hubs were glued in as described in Chapter 4 and the yielding present at this low force is most likely the polyurethane releasing until the bolts set against the bolt holes. The following linear part is interpreted as the linear response of the end fitting.

The nonlinear part at a displacement of 4,25 mm and a load of 67,2 kN is interpreted as the linear load limit for the end fitting. It is clear that some damage must have occurred as the stiffness is reduced. Likewise for the nonlinearity found at 5 mm displacement. If the tube had been unloaded from this point and on it would not have return to its original length.

The maximum load of 96,2 kN can then be seen as a strength reserve towards catastrophic failure. Any overloading past the linear limit do not lead to an instant catastrophic failure. 96,2 kN is 43% more than 67,2 kN and this can be considered a large strength reserve against catastrophic failure.

96,2 kN is 89% of the predicted axial load according to the calculations done in Section 3.8 where the axial load at failure was predicted to 108 kN. A difference of only 11% should be considered very good considering that linear laminate theory is used beyond first ply failure. The maximum load was obtained between the loads where fiber failure in compression, using a cosine distribution, and fiber failure in compression, using a constant bearing load, was predicted. The predictions done using linear laminate theory beyond the first ply failure is in good agreement with the experimental results. Only one test has been performed so it is impossible to determine if this applies to other laminates.

Load proportionality factors calculated for the laminate produced at the maximum load and at the linear load limit is appended in Appendix A for comparison to the design values used in Chapter 2.

When back calculating using Equation 2.4 an axial load of 67,2 kN is found to correspond to the axial load at a pressure of 8,56 MPa. An axial load of 96,2 kN corresponds a pressure of 12,2 MPa.

7.4 Center part

There was only a small difference between the gauges in axial direction in the center of the tube as seen in Figure 6.10. The FEA model has a stiffer behavior than the experimental results.

During the tensile test some bending around an axis going approximately between 90° and 270° is seen from the difference in strain around the circumference at the center of the tube. The difference is 5-7% as seen in Figure 6.11. The bending moment is not very big, but when plotted as a ratio even a small difference is seen. The bending is largest at a displacement of about 1 mm. When comparing to Figure 6.9 it corresponds to the initial compliant part of the test. The bending measured supports the theory about the polyurethane releasing from the hub and the bolts being loaded in an uneven sequence and therefore creating a bending moment in the tube. The bending is fast approaching a constant state after 1 mm displacement. This could be a result of inaccurate alignment of the end fittings in the test machine. This is very likely as the end hubs were modified and welded after the pressure test, as described in Section 5.3.1.

7.5 Bolt area

As seen in Figure 6.3, the FEA model predicts the strain at the midpoint between two bolts to be relatively constant in the middle and rapidly increasing towards the bolts. This indicates that any misalignment of the optical fiber and strain gauges BH2 and BH4 towards any of the bolts is not critical to get good measurements of the strain in the net section. On the other hand the axial strain is changing rapidly with the distance from the tube edge as seen in Figure 6.1. A slight misalignment in that direction could lead to larger errors in the measurements.

The bolt loading response can to be seen in Figure 6.12. The two strain gauges, BH2 and BH4, have almost the same response during loading. This is to be expected, as they are located on each side of the same bolt. The rapid increase in strain at a crosshead displacement of 5 mm corresponds well to the second small nonlinear part seen in Figure 6.9. The sudden increase in strain relates to a sudden increase of the bolt load in the nearby bolts. Load redistribution between the bolts must be happening since the load at the nearby bolts suddenly increased. This is a result of damage being initiated at one or more bolts, decreasing their load bearing capacity and loading other bolts more.

Any increase or decrease in strain at 4,25 mm crosshead displacement related to the elastic load limit cannot be seen in Figure 6.12. The most likely cause of this is the damage relating to the nonlinear behavior is in the other end of the tube. If all net sections had been instrumented with strain gauges, this would be an accurate way to determine the onset of damage as any redistribution of load had been easily detected.

Comparing the FEA force scaled results to the experimental results in Figure 6.12 indicate a more compliant response in the FEA model than in the experimental results.

The optical strain measurements in Figure 6.13 to 6.16 show noise in the measurements. When comparing to FEA results in Figure 6.1 the strains should have smooth transitions around the bolt hole while the optical measurements have larger rapid transitions. The optical fiber was due to the noise unsuitable to measure the load redistribution as the noise was far greater than the strain measurements. The strain gauges gave better results as seen in Figure 6.12. A general trend in the optical measurements is in good agreement with the strain gauge measurements at low displacements, while the optical measurements measure higher strains than the gauges at larger displacements.

7.6 Transition area

It is to note from Figure 6.2 that the hoop strains, according to the FEA model, change rapidly in the transition area. Any misalignment of the mats during production or a slightly misplaced strain gauge could give large errors in the experimental measurements.

The plots in Figure 6.19 and 6.20 shows that the gauges have a linear response. The FEA model has a stiffer response than the experimental results.

The optical fiber measurements of axial strain in the transition is seen in Figure 6.17 to Figure 6.18. The strain is rapidly changing in the transition area as expected from the FEA model.

The strain measured in the optical fiber at the center of the tube correlates well to the strain measured by the strain gauges.

7.7 FEA model compared to experimental results

In Figure 6.21 the percent vice difference between the FEA results and the experimental results is plotted against force. It is clear that the correlation in axial strains at the center are the best with only an underestimation of the strain of 10%. The axial strain at the bolt holes are overestimated with about 50% and the hoop strains in the transition is underestimated with around 30%. This is a clear weakness in the FEA model. It underestimates the strains in hoop direction while the strains near the bolt hole is estimated too high.

Strain measurements from the optical fiber going all the way to the center of the tube is seen in Figure 6.17 to Figure 6.18. Good correlation between the experimental and the force scaled FEA model is seen. The FEA model determine strains with good accuracy only short distances away from the discontinuities in the model. The force scaled FEA results give better results than the displacement scaled results. This is due to the initial yielding as seen in Figure 6.9. The yielding is not taken into account using displacement scaling of the FEA results.

There are numerous possible reasons for the differences between the FEA model and the experimental results. The hoop strains were measured in an area where the thickness of the laminate and the geometry of the shell is changing. It is possibly an inaccurate simplification to use a shell model in this area. The cause of these differences have not been investigated further. The results indicate that such a simple FEA model should be used with caution as it might give to inaccurate predictions.

Chapter 8

Conclusion

Several aspects of the composite tube end fitting have been investigated.

8.1 Production method

The suggested production method produced a good quality tube with a high fiber volume fraction. Winding a helical ply over a mat edge resulted in a volume filled with epoxy underneath the area where the helical ply bridged. A few voids were found in this volume, but in form of small bubbles.

The added mats with an estimated thickness of 1 mm became thinner than expected, only 0,56 mm. This is the main reason for the laminate being thinner than estimated. The estimated thickness of 0,3 mm for the winded plies was in good agreement with the measured average thickness of 0,29 mm.

Bolt holes were drilled with a "glass and tile" drill bit. The result was clean holes without any sign of delamination. The tolerance was larger than expected due to the drill bit being larger than stated on the package.

The liner was applied without any problems, and the method was clean and simple.

8.2 Experimental

A pressure test was conducted and the tube and end fitting leaked at a pressure of 1,3 MPa.

The end fitting had an elastic limit in tension of 67,2 kN corresponding to the axial load at a pressure of 8,56 MPa. A maximum load of 96,2 kN was measured, corresponding to the axial load at a pressure of 12,2 MPa. The maximum load is 89% of the predicted failure load, using laminate theory and the maximum stress criterion beyond first ply failure.

It has not been possible to detect any large skew loading as a result of different bolt behavior. The bolts had uniform damage propagation at both ends of the tube.

The strains predicted by the FEA model is in good agreement with the strains measured in axial direction by the optical fiber, but strains in hoop direction is underestimated and axial strains near the bolt hole is overestimated.

8.3 Further work and suggested improvements to the design

Leakage is serious problem in the end fitting design. The tube is expanding under pressure and a glued interface on the inside of the tube become highly stressed. This expansion of the tube can be utilized to seal the end fitting if an external hub was used. The tube will expand and the laminate will be pushed against an outside hub. If the tube was made as described in

Chapter 3, but with a thicker hoop ply on the outside, this outside ply could be grinded down to a specific diameter and have a high finish quality. This makes the use of standard sealing elements like O-ring seals possible.

As Parker [18] has found, the strength of a bolted joint is increased with 90° ply on the outside of the laminate. As seen in Figure 6.7 the laminate around the bolt holes was pushed upwards on the bolts. If a very thick hoop ply is added on the outside, near the bolts, this deformation could have been limited and the strength increased. As the joint is circular, the laminate has a curvature and this hoop layer could have an even higher beneficial impact on the strength due to the curvature. The ply is easy to make and does not affect an end fitting with an internal hub.

A multi row joint could be investigated a possibly increase the end fitting strength beyond the limit created by yield in the bolts.

A laminate model including damage modeling could be investigated as a tool to avoid the use of linear laminate theory and the maximum stress criterion beyond first ply failure. This might give more accurate strength predictions.

The author has not been able to find any articles about bolted joints in curved or circular laminates. It could been an interesting research project to investigate the influence of laminate curvature on the bolted joint strength.

Bibliography

- [1] C.C. Chamis. Simplified procedures for designing composite bolted joints. *Journal of Reinforced Plastics and Composites*, 9(6):614–626, 1990.
- [2] Tanguy Messenger, Mariusz Pyrz, Bernard Gineste, and Pierre Chauchoot. Optimal laminations of thin underwater composite cylindrical vessels. *Composite Structures*, 58(4):529–537, 2002.
- [3] A Mukherjee and B Varughese. Design guidelines for ply drop-off in laminated composite structures. *Composites Part B: Engineering*, 32(2):153 – 164, 2001. ISSN 1359-8368. doi: 10.1016/S1359-8368(00)00038-X. URL <http://www.sciencedirect.com/science/article/pii/S135983680000038X>.
- [4] Alaattin Aktas and M Husnu Dirikolu. An experimental and numerical investigation of strength characteristics of carbon-epoxy pinned-joint plates. *Composites science and technology*, 64(10):1605–1611, 2004.
- [5] G. Perillo. Internal report at ntnu material properties of hipertex fibres with epicote resin mgs rimr 135 and epikure curing agent rimh 137 in a laminate made with knitted fibres and vacuum assisted resin injection. Internal report in the Composite group at NTNU, 2012.
- [6] Isaac M Daniel, Ori Ishai, Issac M Daniel, and Ishai Daniel. *Engineering mechanics of composite materials*, volume 3. Oxford university press New York, 1994.

-
- [7] Axson Technologies. *Technical Datasheet UR 3435 ISOCYANATE UR 3442 POLYOL POLYURETHANE CASTING ELASTOMER*.
- [8] Michael Chun-Yung Niu. *Composite airframe structures: practical design information and data*. Adaso Adastr Engineering Center, 1992.
- [9] B. Paulshus, T.O. Carlsen, T. Storhaug, and J. M. Johnsen. Composite pipe and a method of manufacturing a composite pipe, 2001.
- [10] Claes-Goran Gustafson and Nils-Petter Vedvik. Interface between a stiff piece and a composite material, a method for the formation of such an interface and a stiff piece therefore, November 15 2011. US Patent 8,056,935.
- [11] Mark James Fahey and Carsten Mueller. End-fittings for composite tubes, method for joining fittings to the ends of composite tubes and composite tubes incorporating end-fitting, September 8 2008. US Patent App. 12/677,159.
- [12] Kenneth J Carstensen, Lawrence P Moore, and John P Biro. Threaded connections utilizing composite materials, April 20 1999. US Patent 5,895,079.
- [13] Derek N Yates and John C Presta. Fiber reinforced composite shaft with metallic connector sleeves mounted by radial pin interlock, January 29 1980. US Patent 4,185,472.
- [14] Craig Tew. Composite drill pipe, July 26 1994. US Patent 5,332,049.
- [15] SJ Dastin. Joining and machining techniques. *Handbook of composites*, 1:602–632, 1982.
- [16] S.W. Tsai. *Composites design*. Think Composites, 1988.
- [17] Pedro Ponces Camanho and Michel Lambert. A design methodology for mechanically fastened joints in laminated composite materials. *Composites Science and Technology*, 66(15):3004–3020, 2006.

- [18] HJ Parker. Effect of stacking sequence and claming force on the bearing stregh of mechanically fastened joints in composite laminates. *Composite Structures*, 53:213–21, 2001.
- [19] Det Norske Veritas. Composite components, 2010.
- [20] Astm d5766 / d5766m - 11 standard test method for open-hole tensile strength of polymer matrix composite laminates, .
- [21] Astm d5961/d5961m-10 standard test method for bearing response of polymer matrix composite laminates, .
- [22] Astm d953-10 standard test method for bearing strength of plastics, .
- [23] Astm d7332/d7332m-09 standard test method for measuring the fastener pull-through resistance of a fiber-reinforced polymer matrix composite, .
- [24] Laszlo P. Kollar and George S. Springer. *Mechanics of Composite Materials*. Cambridge University Press, 2003.
- [25] N.-P. Vedvik. Essential mechanics of composites, 02 2012.
- [26] 3B-Fibreglass, 2012. URL http://www.3b-fibreglass.com/wp-content/themes/3b/pdf/brochures/Brochure%20HiPer-tex_Generic_UK.pdf.
- [27] Devold AMT. *Thecnical Datasheet Devold AMT DBL 800 E10-H*.
- [28] *Technical Data Sheet: EPIKOTE Resin MGS RIMR 135 and EPIKURE Curing Agent MGS RIMH 134 RIMH 137*. Momentive Specialty Chemicals Inc., August 2006.
- [29] H. Hartvigsen, R. Lorentsen, K Michelsen, and S. Seljevoll. *Verkstedhåndboka*. Gyldendal, 1998.
- [30] Rørformet legeme belagt med innvendig slitasjebelegg og framgangsmåte for å framstille et slikt belegg, 2012. URL

- <https://dbsearch2.patentstyret.no/Patent/DetailNewWindow.aspx?idappl=20120721&culture=nb-NO>.
- [31] Fridtjov Irgens. *Formelsamling i mekanikk: statikk, fasthetslære, dynamikk, fluidmekanikk*. Tapir, 1992.
- [32] D.K. Roylance. Netting analysis for filamen-wound pressure vessels. Technical report, Army materials and mechanics research center, Composites division, 1976. URL <http://web.mit.edu/roylance/www/netting.pdf>.
- [33] L Ingvar Eriksson. Contact stresses in bolted joints of composite laminates. *Composite Structures*, 6(1):57–75, 1986.
- [34] LJ Hart-Smith. Mechanically-fastened joints for advanced composites phenomenological considerations and simple analyses. In *Fibrous Composites in Structural Design*, pages 543–574. Springer, 1980.
- [35] S.T.Peters, editor. *Composite Filament Winding*. ASM International, 2011.
- [36] L. Zhao, S.C. Mantell, D. Cohen, and R. McPeak. Finite element modeling of the filament winding process. *Composite structures*, 52(3): 499–510, 2001.
- [37] Zywx Inc. *FLEX-Z 3 Product Data Sheet / User Manual*, 2013.
- [38] Srinivasa D Thoppul, Joana Finegan, and Ronald F Gibson. Mechanics of mechanically fastened joints in polymer–matrix composite structures—a review. *Composites Science and Technology*, 69(3):301–329, 2009.
- [39] S.Y. Lee and G.S. Springer. Filament winding cylinders i. process model. *Journal of composite materials*, 24(12):1270–1298, 1990.
- [40] *Abaqus 6.11 Documentation Collection*. Simulia Corp.

-
- [41] Alaattin Aktaş, Hüseyin İmrek, and Yusuf Cunedioğlu. Experimental and numerical failure analysis of pinned-joints in composite materials. *Composite structures*, 89(3):459–466, 2009.
- [42] Magnus Lund Håheim. Health monitoring of composites using optical fibres. Master’s thesis, Norwegian University of Science and Technology, 2012.
- [43] TML. *TML Series F Strain Gauges*. URL http://www.tml.jp/e/product/strain_gauge/catalog_pdf/Fseries.pdf.

Appendix A

Tables

TABLE A.1: Sample tube layup as estimated. Inside ply to the bottom.

A		B		C		D		E	
Material	Angle	Material	Angle	Material	Angle	Material	Angle	Material	Angle
Tick.	Tick.	Tick.	Tick.	Tick.	Tick.	Tick.	Tick.	Tick.	Tick.
Hip.Tex.	90							Hip.Tex.	90
	0,30								0,30
Hip.Tex.	90							E-glass	45
	0,30								0,24
Hip.Tex.	90							E-glass	-45
	0,30								0,24
Hip.Tex.	90							Hip.Tex.	0
	0,30								0,51
Hip.Tex.	90							Hip.Tex.	90
	0,30								0,30
Hip.Tex.	90							E-glass	45
	0,30								0,24
Hip.Tex.	90							E-glass	-45
	0,30								0,24
Hip.Tex.	90							E-glass	0
	0,30								0,51
Hip.Tex.	90							Hip.Tex.	90
	0,30								0,30
Hip.Tex.	90							E-glass	45
	0,30								0,24
Hip.Tex.	90							E-glass	-45
	0,30								0,24
Hip.Tex.	90							E-glass	0
	0,30								0,51
Hip.Tex.	90							Hip.Tex.	±12,7
	0,30								7
Hip.Tex.	90							Hip.Tex.	±12,7
	0,30								7
Hip.Tex.	90							E-glass	0
	0,30								0,51
Hip.Tex.	90							E-glass	45
	0,30								0,24
Hip.Tex.	90							E-glass	-45
	0,30								0,24
Hip.Tex.	90							Hip.Tex.	90
	0,30								0,30
Total ticness	1,80	Total ticness	2,80	Total ticness	3,80	Total ticness	4,8	Total ticness	5,8

TABLE A.2: Sample tube layup as produced. Inside ply to the bottom.

A		B		C		D		E	
Material	Angle	Material	Angle	Material	Angle	Material	Angle	Material	Angle
Tick.		Tick.		Tick.		Tick.		Tick.	
Hip.Tex.	90							Hip.Tex.	90
	0,29								0,29
Hip.Tex.	90							E-glass	45
	0,29								0,14
Hip.Tex.	90							E-glass	-45
	0,29								0,14
Hip.Tex.	90							E-glass	0
	0,29								0,29
Hip.Tex.	90							Hip.Tex.	90
	0,29								0,29
Hip.Tex.	90							E-glass	45
	0,29								0,14
Hip.Tex.	90							E-glass	-45
	0,29								0,14
Hip.Tex.	90							E-glass	0
	0,29								0,29
Hip.Tex.	90							Hip.Tex.	90
	0,29								0,29
Hip.Tex.	90							E-glass	45
	0,29								0,14
Hip.Tex.	90							E-glass	-45
	0,29								0,14
Hip.Tex.	90							Hip.Tex.	90
	0,29								0,29
Total ticsness	1,74	Total ticsness	2,30	Total ticsness	2,87	Total ticsness	3,4275	Total ticsness	3,99

TABLE A.3: Load proportionality factors for the produced laminate at maximum load obtained during tensile testing.

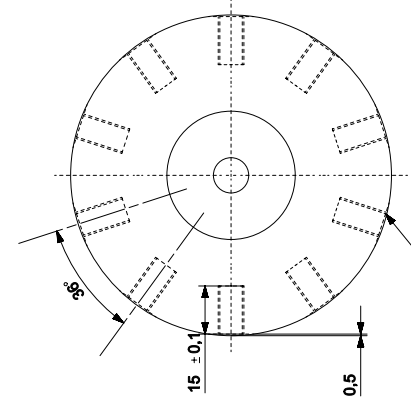
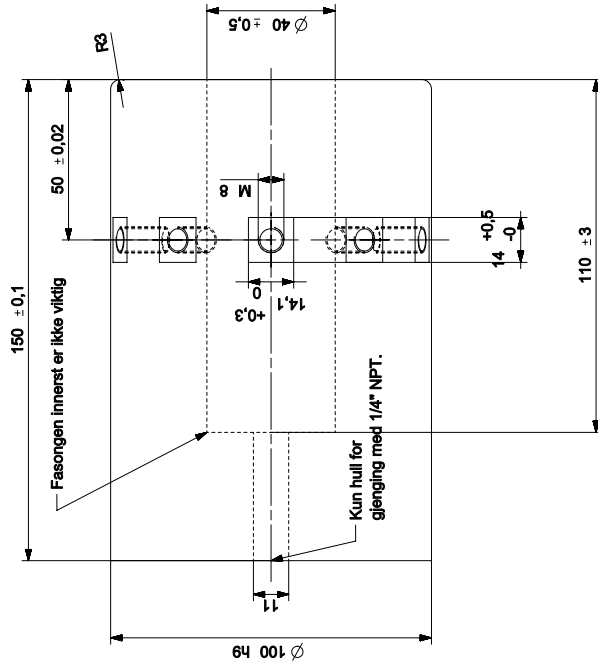
Ply nr	Angle [deg]	Bearing load constant		Bearing load cosine		Net section $K_t = 4$		Net section $K_t = 3$		Shear out out		Wedge splitting	
		f	Exceeded	f	Exceeded	f	Exceeded	f	Exceeded	f	Exceeded	f	Exceeded
1	90	0,60		0,95		3,23	Y_T	2,43	Y_T	0,27		0,12	
2	-45	0,44		0,69		1,69	Y_T	1,27	Y_T	0,39		0,38	
3	45	0,45		0,71		1,75	Y_T	1,31	Y_T	0,12		0,36	
4	0	0,51		0,80		0,52		0,39		0,19		0,65	
5	12,7	0,70		1,11	X_C	0,64		0,48		0,24		0,60	
6	-12,7	0,74		1,16	X_C	0,66		0,50		0,24		0,59	
7	0	0,58		0,91		0,59		0,44		0,19		0,61	
8	-45	0,53		0,83		2,24	Y_T, S_{XY}	1,68	Y_T	0,38		0,32	
9	45	0,54		0,85		2,29	Y_T, S_{XY}	1,72	Y_T	0,11		0,32	
10	90	0,83		1,30	S_{XY}	4,45	Y_T	3,34	Y_T	0,26		0,10	
11	0	0,65		1,02	X_C	0,66		0,50		0,18		0,56	
12	-45	0,58		0,91		2,57	Y_T, S_{XY}	1,93	Y_T	0,37		0,29	
13	45	0,59		0,93		2,62	Y_T, S_{XY}	1,96	Y_T	0,11		0,29	
14	90	0,93		1,46	Y_C	4,97	Y_T	3,73	Y_T	0,26		0,09	
15	0	0,72		1,13	X_C	0,73		0,55		0,18		0,51	
16	-45	0,63		1,00	S_{XY}	2,90	Y_T, S_{XY}	2,17	Y_T	0,37		0,25	
17	45	0,64		1,01	S_{XY}	2,94	Y_T, S_{XY}	2,21	Y_T	0,11		0,26	
18	90	1,02	Y_C	1,61	Y_C	5,49	Y_T	4,12	Y_T	0,26		0,09	

TABLE A.4: Load proportionality factors for the produced laminate at the linear limit load found during tensile testing.

Ply nr	Angle [deg]	Bearing load constant		Bearing load cosine		Net section $K_t = 4$		Net section $K_t = 3$		Shear out out		Wedge splitting	
		f	Exceeded	f	Exceeded	f	Exceeded	f	Exceeded	f	Exceeded	f	Exceeded
1	90	0,42		0,66		2,26	Y_T	1,70	Y_T	0,19		0,082672	
2	-45	0,31		0,48		1,18	Y_T	0,89		0,27		0,26575	
3	45	0,31		0,49		1,22	Y_T	0,92		0,08		0,252252	
4	0	0,36		0,56		0,36		0,27		0,13		0,45523	
5	12,7	0,49		0,77		0,44		0,33		0,17		0,419353	
6	-12,7	0,51		0,81		0,46		0,35		0,17		0,411607	
7	0	0,41		0,64		0,41		0,31		0,13		0,422955	
8	-45	0,37		0,58		1,57	Y_T	1,18	Y_T	0,26		0,225723	
9	45	0,38		0,59		1,60	Y_T	1,20	Y_T	0,08		0,22038	
10	90	0,58		0,91		3,11	Y_T	2,33	Y_T	0,18		0,070427	
11	0	0,46		0,72		0,46		0,35		0,13		0,391238	
12	-45	0,41		0,64		1,80	Y_T	1,35	Y_T	0,26		0,201861	
13	45	0,41		0,65		1,83	Y_T	1,37	Y_T	0,08		0,201379	
14	90	0,65		1,02	Y_C	3,48	Y_T	2,61	Y_T	0,18		0,065195	
15	0	0,50		0,79		0,51		0,38		0,13		0,359522	
16	-45	0,44		0,70		2,03	Y_T	1,52	Y_T	0,26		0,177998	
17	45	0,45		0,71		2,06	Y_T	1,54	Y_T	0,08		0,182378	
18	90	0,72		1,12	Y_C	3,84	Y_T	2,88	Y_T	0,18		0,059963	

Appendix B

Hub drawing



Alle hullene er ikke og fordelt med 36 grader i mellom seg. Gjengelapp kan brukes, tenkt gjenget så langt det går når hulltet er boret 15mm. Fasong i bunnen av hullene er ikke viktig.

Matriale: Stål
 Ved spørsmål kontakt:
 Karsten Doris
 karsted@stud.ntnu.no
 +47 95943135

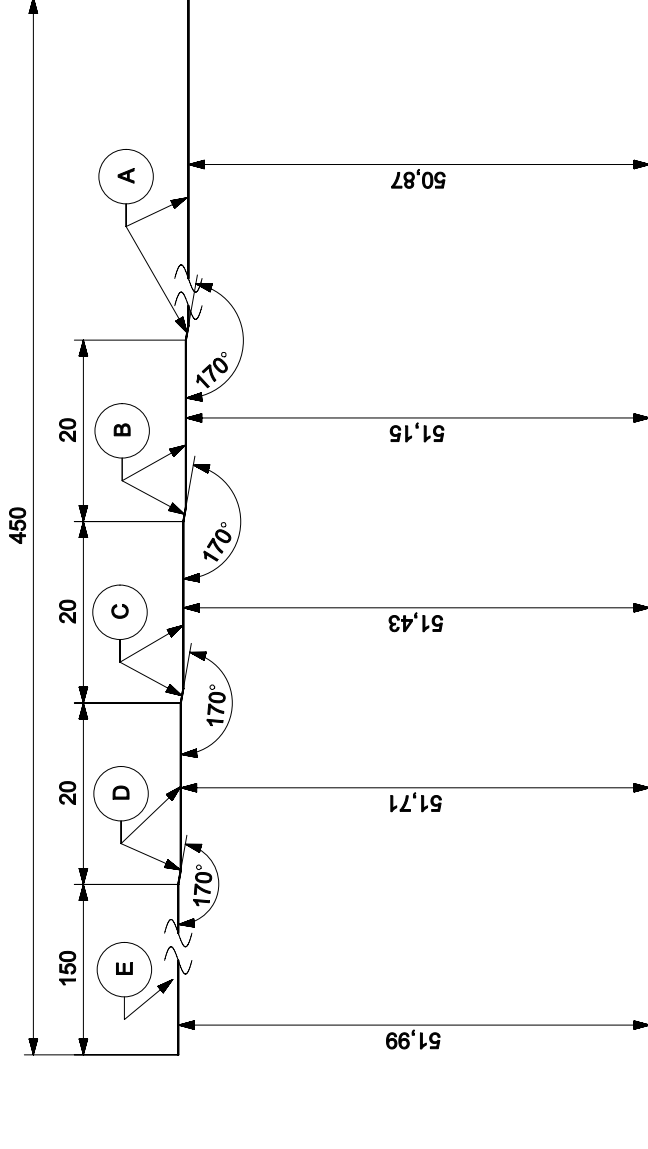
Det viktige her er at hullene og flatene står normalt på yttersiden av sylindere og at planet de danner er normalt på senteraksen.

Utvendig trengs det finmaskinering men innvendig holder grovmaskinering

Appendix C

FEA shell drawing

FEA Shell



Appendix D

HSE forms

**Sikkerhets- og kvalitetsgjennomgang av
laboratorietester og verkstedsarbeid**
**Safety and Quality Evaluation of Activities in
the Laboratory and Workshop**



Perleporten

1 Identifikasjon - Identification		Dokumentnr. - Document no.:	
Kundenavn - Customer name Karsten Dons	Prosjektnavn - Project name Filament winding	Prosjektnr. - Project no. 69450723	
Beskrivelse av arbeid - Description of job Liner application with Axson UR 3435/3442			Dato - Date 30.4-10.06.13
2 Prosjekt - Team			
Prosjektleder og organisasjon - Project manager and organization	Karsten Dons	Ansvarlig for instrumentering - Responsible for instrumentation.	Karsten Dons
Leiestedsansvarlig - Laboratory responsible		Operator - Operator	Karsten Dons
Auditor for sikkerhets og kvalitetsgjennomgang - Auditor for safety check	Andreas Echtermeyer	Ansvarlig for styring av forsøk - Responsible for running the experiment.	Karsten Dons
Ansvarlig for eksperimentelt faglig innhold - Responsible for experimental and scientific content	Karsten Dons	Ansvarlig for logging av forsøksdata - Responsible for logging and storing experimental data	Karsten Dons
Ansvarlig for dimensjonering av last og trykkpåkjennte komponenter - Responsible for dimensioning load bearing and pressurized components	-	Ansvarlig for montering av testrigg - Responsible for building the rig	Karsten Dons
3 Viktig!! - Important!!			J: Ja - Yes / N: Nei - No
Er arbeidsordren signert? - Is the work order signed?			Yes
Trenger operatoren kurs i bruk av maskinen(e)? - Does the operator need training on the equipment?			Yes
Har operatoren sikkerhetskurs? (påbudt) - Has the operator followed the safety courses? (mandatory)			Yes
4.1 Sikkerhet - Safety (Testen medfører - The test contains)			J: Ja - Yes / N: Nei - No
Stor last - Big loads	No	Brannfare - Danger of fire	No
Tunge løft - Heavy lifting	No	Arbeid i høyden - Working at heights	No
Hengende last - Hanging load	No	Hydraulisk trykk - Hydraulic pressure	No
Gasstrykk - Gas pressure	No	Vanntrykk - Water pressure	No
Høy temperatur - High temperature	No	Lav temperatur - Low temperature	No
Deler i høy hastighet - Parts at high velocity	Yes	Farlige kjemikalier - Dangerous chemicals	Yes
Sprutakselerasjon ved brudd - Sudden acceleration at fracture/failure	Yes	Forspente komponenter - Pre-tensioned components	No
Farlig støv - Dangerous dust	No	Kraftig støy - Severe noise	No
Klemfare - Danger of pinching	No	Roterende deler - Rotating parts	No
4.2 Påkrevet verneutstyr - Required safety equipment			J: Ja - Yes / N: Nei - No
Briller (påbudt) - Glasses (mandatory)	Yes	Vernesko - Safet shoes	Yes
Hjelm - Helmet	No	Hansker - Gloves	Yes
Skjerm - Screen	No	Visir - Visir	No
Hørselsvern - Earprotection	No	Løfteredskap - Lifting equipment	No
Yrkessele, fällsele, etc. - Harness ropes, other measures to prevent falling down.	No		

Sikkerhets- og kvalitetsgjennomgang av laboratorietester og verkstedsarbeid



5.1 Beskrivelse av aktivitet – Description of the activity (see Appendix)

Vurdering skal være basert på en skriftlig prosedyre for bruk av maskinen. I enkelte tilfeller kan prosedyre bli beskrevet direkte i tabellen nedenfor.

The evaluation shall be based on a written operating procedure for the machine. For simple cases the procedure can be directly described in the tables below.

Nr.	Beskrivelse av aktivitet – Description of activity	Fare – Danger	Prosedyre nr. – Procedure no.	Samsynlighet – Probability	Konsekvens – Consequence	Risiko – Risk
1	Rotomolding polyurethane inside test tube in a lathe at high RPM.	Leakage and spill of polyurethane Pipe chatters	1 2	3 2	2 3	6 6

5.2 Korrigerende Tiltak – Corrective Actions

Korrigerende tiltak – Corrective action

The evaluation shall be based on a written operating procedure for the machine. For simple cases the procedure can be directly described in the tables below.

Nr.	Beskrivelse av aktivitet – Description of activity	Fare – Danger	Prosedyre nr. – Procedure no.	Samsynlighet – Probability	Konsekvens – Consequence	Risiko – Risk	Utført dato – Date of action
1	Seal pipe off with tape, start with slow rotation, wear protective glasses and cover up machine before starting.			1	2	2	16.4.13
2	Start with slow rotation and look for any instability, wear protective glasses, do not stand in directly in front of lathe.			1	2	2	16.4.13

Sikkerhets og kvalitetsgjennomgang av laboratorietester og verkstedsarbeid



5.3 Feilkilder – Reasons for mistakes/errors

Sjekkliste: Er følgende feilkilder vurdert? – Check list: Is the following considered?

J: Ja – Yes / N: Nei – No

Tap av strøm – <i>Loss of electricity</i>	No	Overspenning – <i>Voltage surge</i>	No
Elektromagnetisk støy – <i>Electromagnetic noise</i>	No	Manglende aggregatkapasitet av hydraulikk – <i>Insufficient power of the machine</i>	No
Jordfeil – <i>Electrical earth failure</i>	No	Vannsprut – <i>Water jet</i>	No
Ustabil trykk av hydraulikk/kraft – <i>Unstable pressure or hydraulic force</i>	No	Tilfeldig avbrudd av hydraulikk/kraft – <i>Unintended interruption of power supply</i>	No
Last-/ forskyvnings grenser etablert? – <i>Are load and displacement limits established?</i>	No	Lekkasjer (slanger/koblinger, etc.) – <i>Leakage of pipes, hoses, joints, etc.</i>	No
Mulige påvirkninger fra andre aktiviteter – <i>Possible interference from other activities</i>	Yes	Mulige påvirkninger på andre aktiviteter – <i>Possible interference towards other activities</i>	Yes
Problemer med datalogging og lagring – <i>Troubles in loading and storage</i>	No	Brann i laboratoriet – <i>Fire in the laboratory</i>	No

6 Kalibreringsstatus for utstyr – Calibration of equipment

(ex: load cell, extensometer, pressure transducer, etc)

I.D.	Utstyr - Equipment	Gyldig til (dato) – Valid until (date)

7 Sporbarhet – Traceability

Ekstisterer – *Is there*

J: Ja – Yes / N: Nei – No

Er alle provematerialene kjente og identifiserbare? – <i>Are all experimental materials known and traceable?</i>	Yes
Ekstisterer det en plan for markering av alle prøvene? – <i>Is there a plan for marking all specimens?</i>	Yes
Er dataloggingsutstyret identifisert? – <i>Is the data acquisition equipment identified?</i>	-
Er originaldata lagret uten modifikasjon? – <i>Is the original data stored safely without modification?</i>	-
Ekstisterer det en backup-prosedyre? – <i>Is there a back-up procedure for the data (hard disk crash)?</i>	-
Ekstisterer det en plan for lagring av provestykker etter testing? – <i>Is there a plan for storing samples after testing?</i>	-
Ekstisterer en plan for avhending av gamle provestykker? – <i>Is there a plan for disposing of old samples?</i>	Yes

8 Kommentarer – Comments

9 Signaturer – Signatures

Godkjent (dato/sign) – Approved (date/signature)

Prosjektleder – Project leader	Verifikatør – Verifier	Godkjent – Approved by

Sikkerhets- og kvalitetsgjennomgang av laboratorietester og verkstedsarbeid

Safety and Quality Evaluation of Activities in the Laboratory and Workshop



Perleporten

1 Identifikasjon - Identification		Dokumentnr. - Document no.:	
Kundenavn – Customer name Karsten Dons	Prosjektnavn – Project name Filament winding	Prosjektnr. – Project no. 69450723	
Beskrivelse av arbeid – Description of job Pressure test of fiberglass tube		Dato – Date 30.4-10.06.13	
2 Prosjekt - Team			
Prosjektleder og organisasjon – <i>Project manager and organization</i>	Karsten Dons	Ansvarlig for instrumentering – <i>Responsible for instrumentation.</i>	Karsten Dons
Leiestedsansvarlig – <i>Laboratory responsible</i>		Operatør – <i>Operator</i>	Karsten Dons
Auditør for sikkerhets og kvalitetsgjennomgang – <i>Auditor for safety check</i>	Andreas Echtermeyer	Ansvarlig for styring av forsøk – <i>Responsible for running the experiment.</i>	Karsten Dons
Ansvarlig for eksperimentelt faglig innhold – <i>Responsible for experimental and scientific content</i>	Karsten Dons	Ansvarlig for logging av forsøksdata – <i>Responsible for logging and storing experimental data</i>	Karsten Dons
Ansvarlig for dimensjonering av last og trykkpåkjenne komponenter – <i>Responsible for dimensioning load bearing and pressurized components</i>	– KARSTEN DONS	Ansvarlig for montering av testrigg – <i>Responsible for building the rig</i>	Karsten Dons
3 Viktig!! – Important!!			J: Ja – Yes / N: Nei – No
Er arbeidsordren signert? – <i>Is the work order signed?</i>			Yes
Trenger operatøren kurs i bruk av maskinen(e)? – <i>Does the operator need training on the equipment?</i>			Yes
Har operatøren sikkerhetskurs? (påbudt) – <i>Has the operator followed the safety courses? (mandatory)</i>			Yes
4.1 Sikkerhet – Safety (Testen medfører – <i>The test contains</i>)		J: Ja – Yes / N: Nei – No	
Stor last – <i>Big loads</i>	No	Brannfare – <i>Danger of fire</i>	No
Tunge løft – <i>Heavy lifting</i>	No	Arbeid i høyden – <i>Working at heights</i>	No
Hengende last – <i>Hanging load</i>	No	Hydraulisk trykk – <i>Hydraulic pressure</i>	No
Gasstrykk – <i>Gas pressure</i>	No	Vanntrykk – <i>Water pressure</i>	Yes
Høy temperatur – <i>High temperature</i>	No	Lav temperatur – <i>Low temperature</i>	No
Deler i høy hastighet – <i>Parts at high velocity</i>	No	Farlige kjemikalier – <i>Dangerous chemicals</i>	No
Sprutakseleksjon ved brudd – <i>Sudden acceleration at fracture/failure</i>	Yes	Forspente komponenter – <i>Pre-tensioned components</i>	No
Farlig støv – <i>Dangerous dust</i>	No	Kraftig støy – <i>Severe noise</i>	No
Klemfare – <i>Danger of pinching</i>	No	Roterende deler – <i>Rotating parts</i>	No
4.2 Påkrevet verneutstyr – Required safety equipment		J: Ja – Yes / N: Nei – No	
Briller (påbudt) – <i>Glasses (mandatory)</i>	Yes	Vernesko – <i>Safet shoes</i>	Yes
Hjelm – <i>Helmet</i>	No	Hansker – <i>Gloves</i>	Yes
Skjerm – <i>Screen</i>	Yes	Visir – <i>Visir</i>	No
Hørselsvern – <i>Earprotection</i>	No	Løfteredskap – <i>Lifting equipment</i>	No
Yrkessele, fallsele, etc. – <i>Harness ropes, other measures to prevent falling down.</i>	No		

Sikkerhets og kvalitetsgjennomgang av laborietester og verkstedsarbeid



5.3 Feilkilder – Reasons for mistakes/errors			
Sjekkliste: Er følgende feilkilder vurdert? – Check list: Is the following considered? J: Ja – Yes / N: Nei - No			
Tap av strøm – Loss of electricity	No	Overspenning – Voltage surge	No
Elektromagnetisk støy – Electromagnetic noise	No	Manglende aggregatkapasitet av hydraulikk – Insufficient power of the machine	No
Jordfeil – Electrical earth failure	No	Vannsprut – Water jet	No
Ustabil trykk av hydraulikk/kraft – Unstable pressure or hydraulic force	No	Tilfeldig avbrudd av hydraulikk/kraft – Unintended interruption of power supply	No
Last-/ forskyvnings grenser etablert? – Are load and displacement limits established?	No	Lekkasjer (slanger/koblinger, etc.) – Leakage of pipes, hoses, joints, etc.	No
Mulige påvirkninger fra andre aktiviteter – Possible interference from other activities	Yes	Mulige påvirkninger på andre aktiviteter – Possible interference towards other activities	Yes
Problemer med datalogging og lagring – Troubles in loading and storage	No	Brann i laboratoriet – Fire in the laboratory	No
6 Kalibreringsstatus for utstyr – Calibration of equipment (ex: load cell, extensometer, pressure transducer, etc)			
I.D.	Utstyr - Equipment	Gyldig til (dato) – Valid until (date)	
7 Sporbarhet – Traceability			
Eksisterer – Is there J: Ja – Yes / N: Nei - No			
Er alle prøvematerialene kjente og identifiserbare? – Are all experimental materials known and traceable?		Yes	
Eksisterer det en plan for markering av alle prøvene? – Is there a plan for marking all specimens?		Yes	
Er dataloggingsutstyret identifisert? – Is the data acquisition equipment identified?		Yes	
Er originaldata lagret uten modifikasjon? – Is the original data stored safely without modification?		Yes	
Eksisterer det en backup-prosedyre? – Is there a back-up procedure for the data (hard disk crash)?		Yes	
Eksisterer det en plan for lagring av prøvestykker etter testing? – Is there a plan for storing samples after testing?		Yes	
Eksisterer en plan for avhending av gamle prøvestykker? – Is there a plan for disposing of old samples?		Yes	
8 Kommentarer – Comments			
9 Signaturer – Signatures			
Godkjent (dato/sign) – Approved (date/signature)			
Prosjektleder – Project leader	Verifikatør – Verifier	Godkjent – Approved by	

**Sikkerhets- og kvalitetsgjennomgang av
laboratorietester og verkstedsarbeid**
**Safety and Quality Evaluation of Activities in
the Laboratory and Workshop**



Perleporten

1 Identifikasjon - Identification		Dokumentnr. - Document no.:	
Kundenavn - Customer name Karsten Dons	Prosjektnavn - Project name Filament winding	Prosjektnr. - Project no. 69450723	
Beskrivelse av arbeid - Description of job Tensile test of composite tube		Dato - Date 15.5.13-10.06.13	
2 Prosjekt - Team			
Prosjektleder og organisasjon - Project manager and organization	Karsten Dons	Ansvarlig for instrumentering - Responsible for instrumentation.	Karsten Dons
Leiestedsansvarlig - Laboratory responsible		Operatør - Operator	Karsten Dons
Auditør for sikkerhets og kvalitetsgjennomgang - Auditor for safety check	Andreas Echtermeyer	Ansvarlig for styring av forsøk - Responsible for running the experiment.	Karsten Dons
Ansvarlig for eksperimentelt faglig innhold - Responsible for experimental and scientific content	Karsten Dons	Ansvarlig for logging av forsøksdata - Responsible for logging and storing experimental data	Karsten Dons
Ansvarlig for dimensjonering av last og trykkpåkjenne komponenter - Responsible for dimensioning load bearing and pressurized components	Karsten Dons	Ansvarlig for montering av testrigg - Responsible for building the rig	Karsten Dons
3 Viktig!! - Important!!			
Er arbeidsordren signert? - Is the work order signed?			J: Ja - Yes / N: Nei - No Yes
Trenger operatøren kurs i bruk av maskinen(e)? - Does the operator need training on the equipment?			Yes
Har operatøren sikkerhetskurs? (påbudt) - Has the operator followed the safety courses? (mandatory)			Yes
4.1 Sikkerhet - Safety (Testen medfører - The test contains)			
			J: Ja - Yes / N: Nei - No
Stor last - Big loads	Yes	Brannfare - Danger of fire	No
Tunge løft - Heavy lifting	Yes	Arbeid i høyden - Working at heights	No
Hengende last - Hanging load	No	Hydraulisk trykk - Hydraulic pressure	No
Gasstrykk - Gas pressure	No	Vanntrykk - Water pressure	No
Høy temperatur - High temperature	No	Lav temperatur - Low temperature	No
Deler i høy hastighet - Parts at high velocity	No	Farlige kjemikalier - Dangerous chemicals	No
Sprutakselerasjon ved brudd - Sudden acceleration at fracture/failure	Yes	Forspente komponenter - Pre-tensioned components	No
Farlig støv - Dangerous dust	No	Kraftig støy - Severe noise	No
Klemfare - Danger of pinching	No	Roterende deler - Rotating parts	No
4.2 Påkrevet verneutstyr - Required safety equipment			
			J: Ja - Yes / N: Nei - No
Briller (påbudt) - Glasses (mandatory)	Yes	Vernesko - Safet shoes	Yes
Hjelm - Helmet	No	Hansker - Gloves	No
Skjerm - Screen	No	Visir - Visir	No
Hørselsvern - Earprotection	No	Løfteredskap - Lifting equipment	No
Yrkesele, fallsele, etc. - Harness ropes, other measures to prevent falling down.	No		

Sikkerhets og kvalitetsgjennomgang av laboratorietester og verkstedsarbeid



5.3 Feilkilder – Reasons for mistakes/errors		
Sjekkliste: Er følgende feilkilder vurdert? – Check list: Is the following considered? J: Ja – Yes / N: Nei – No		
Tap av strøm – Loss of electricity	No	Overspenning – Voltage surge
Elektromagnetisk støy – Electromagnetic noise	No	Manglende aggregatkapasitet av hydraulikk – Insufficient power of the machine
Jordfeil – Electrical earth failure	No	Vannsprut – Water jet
Ustabil trykk av hydraulikk/kraft – Unstable pressure or hydraulic force	No	Tilfeldig avbrudd av hydraulikk/kraft – Unintended interruption of power supply
Last-/ forskyvnings grenser etablert? – Are load and displacement limits established?	No	Lekkasjer (slanger/koblinger, etc.) – Leakage of pipes, hoses, joints, etc.
Mulige påvirkninger fra andre aktiviteter – Possible interference from other activities	Yes	Mulige påvirkninger på andre aktiviteter – Possible interference towards other activities
Problemer med datalogging og lagring – Troubles in loading and storage	No	Brann i laboratoriet – Fire in the laboratory
6 Kalibreringsstatus for utstyr – Calibration of equipment (ex: load cell, extensometer, pressure transducer, etc)		
I.D.	Utstyr - Equipment	Gyldig til (dato) – Valid until (date)
7 Sporbarhet – Traceability		
Eksisterer – Is there J: Ja – Yes / N: Nei – No		
Er alle prøvematerialene kjente og identifiserbare? – Are all experimental materials known and traceable?		Yes
Eksisterer det en plan for markering av alle prøvene? – Is there a plan for marking all specimens?		Yes
Er dataloggingsutstyret identifisert? – Is the data acquisition equipment identified?		Yes
Er originaldata lagret uten modifikasjon? – Is the original data stored safely without modification?		Yes
Eksisterer det en backup-prosedyre? – Is there a back-up procedure for the data (hard disk crash)?		Yes
Eksisterer det en plan for lagring av prøvestykker etter testing? – Is there a plan for storing samples after testing?		Yes
Eksisterer en plan for avhending av gamle prøvestykker? – Is there a plan for disposing of old samples?		Yes
8 Kommentarer – Comments		
9 Signaturer – Signatures		
Godkjent (dato/sign) – Approved (date/signature)		
Prosjektleder – Project leader	Verifikatør – Verifier	Godkjent – Approved by